Article

Developmental Cell

De novo generation of macrophage from placenta-derived hemogenic endothelium

Graphical abstract

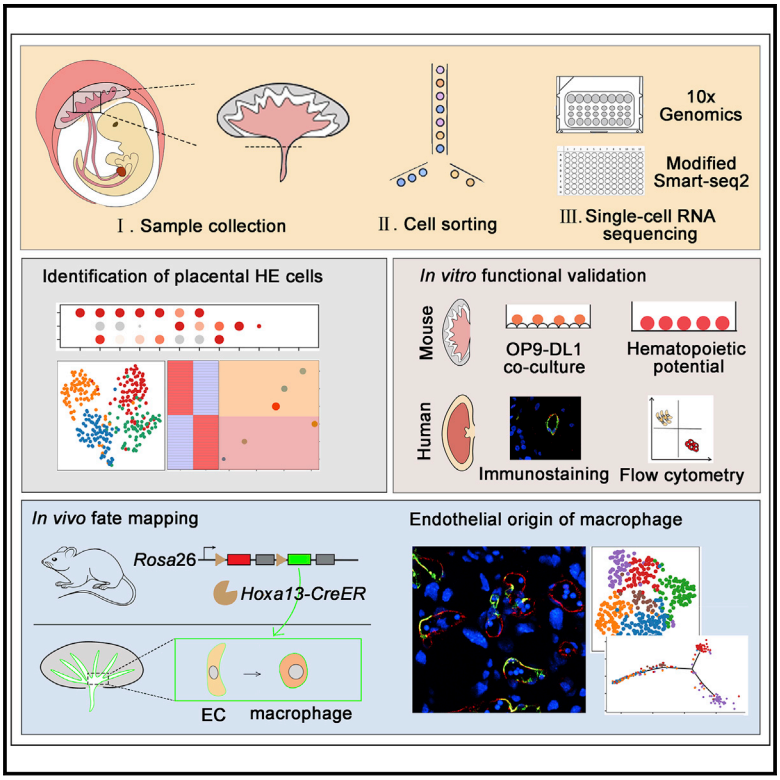

Highlights

- Single-cell transcriptional atlas of placental hematopoiesis in mouse embryos
- Identification of a subset of placental ECs with hemogenic potential
- *Hoxa13*-mediated fate mapping of macrophage *de novo* generation from ECs
- Transcriptomic characterization of HBC-like cells in fetal placental labyrinth

Authors

Guixian Liang, Chunyu Zhou, Xiangxiang Jiang, ..., Hongmei Wang, Jing-Dong J. Han, Feng Liu

Correspondence

bg200@cam.ac.uk (B.G.), wanghm@ioz.ac.cn (H.W.), jackie.han@pku.edu.cn (J.-D.J.H.), liuf@ioz.ac.cn (F.L.)

In brief

Using single-cell RNA sequencing and lineage tracing, Liang et al. profile the transcriptional landscape of mouse fetal placental hematopoiesis and uncover that Hoxa13-labeled ECs can produce placental macrophages, named Hofbauer cell (HBC)-like cells, highlighting the placenta as a source of macrophages.

Liang et al., 2021, Developmental Cell *56*, 2121–2133
July 26, 2021
https://doi.org/10.1016/j.devcel.2021.06.005

CellPress

Developmental Cell

CellPress

Article

De novo generation of macrophage from placenta-derived hemogenic endothelium

Guixian Liang,[1,2,7,9] Chunyu Zhou,[3,9] Xiangxiang Jiang,[2,5,9] Yifan Zhang,[1,2,7] Baofeng Huang,[1,2,7] Suwei Gao,[1,2,7] Zhixin Kang,[1,2,7] Dongyuan Ma,[1,2] Fengchao Wang,[6] Berthold Gottgens,[8,*] Hongmei Wang,[2,5,7,*] Jing-Dong J. Han,[3,4,*] and Feng Liu[1,2,7,10,*]

[1]State Key Laboratory of Membrane Biology, Institute of Zoology, Chinese Academy of Sciences, Beijing 100101, China
[2]Institute for Stem Cell and Regeneration, Chinese Academy of Sciences, Beijing 100101, China
[3]CAS Key Laboratory of Computational Biology, Shanghai Institute of Nutrition and Health, University of Chinese Academy of Sciences, Chinese Academy of Sciences, Shanghai 200031, China
[4]Peking-Tsinghua Center for Life Sciences, Academy for Advanced Interdisciplinary Studies, Center for Quantitative Biology (CQB), Peking University, Beijing 100871, China
[5]State Key Laboratory of Stem Cell and Reproductive Biology, Institute of Zoology, Chinese Academy of Sciences, Beijing 100101, China
[6]National Institute of Biological Sciences, Beijing 102206, China
[7]University of Chinese Academy of Sciences, Beijing 100049, China
[8]Department of Haematology, Wellcome & MRC Cambridge Stem Cell Institute, University of Cambridge, Cambridge CB2 0AW, UK
[9]These authors contributed equally
[10]Lead contact
*Correspondence: bg200@cam.ac.uk (B.G.), wanghm@ioz.ac.cn (H.W.), jackie.han@pku.edu.cn (J.-D.J.H.), liuf@ioz.ac.cn (F.L.)
https://doi.org/10.1016/j.devcel.2021.06.005

SUMMARY

Macrophages play pivotal roles in immunity, hematopoiesis, and tissue homeostasis. In mammals, macrophages have been shown to originate from yolk-sac-derived erythro-myeloid progenitors and aorta-gonad-mesonephros (AGM)-derived hematopoietic stem cells. However, whether macrophages can arise from other embryonic sites remains unclear. Here, using single-cell RNA sequencing, we profile the transcriptional landscape of mouse fetal placental hematopoiesis. We uncover and experimentally validate that a CD44$^+$ subpopulation of placental endothelial cells (ECs) exhibits hemogenic potential. Importantly, lineage tracing using the newly generated *Hoxa13* reporter line shows that *Hoxa13*-labeled ECs can produce placental macrophages, named Hofbauer cell (HBC)-like cells. Furthermore, we identify two subtypes of HBC-like cells, and cell-cell interaction analysis identifies their potential roles in angiogenesis and antigen presentation, separately. Our study provides a comprehensive understanding of placental hematopoiesis and highlights the placenta as a source of macrophages, which has important implications for both basic and translational research.

INTRODUCTION

Placenta is a critical organ for embryo development in the uterus (Rossant and Cross, 2001). It originates from the extra-embryonic trophectoderm and intra-embryonic mesodermal tissues, including chorionic mesoderm and allantois, which gives rise to the fetal placental vasculature (Rossant and Cross, 2001; Downs, 2002). In addition to its role in maternal-fetal communication, placenta has been shown to serve as a hematopoietic organ during embryogenesis (Lee et al., 2010; Gekas et al., 2005; Ottersbach and Dzierzak, 2005; Alvarez-Silva et al., 2003; Gekas et al., 2010). For example, CD41$^+$ hematopoietic cells are observed in the placenta of *Ncx1* mutant embryos that lack blood circulation, implying that placenta could generate hematopoietic cells *de novo* (Rhodes et al., 2008; Koushik et al., 2001). However, the lethality of *Ncx1* mutation in embryos at E11.5 hinders further investigation of the biological function of placenta-resident hematopoietic cells.

It is generally believed that definitive hematopoietic cells are derived from hemogenic endothelial (HE) cells, a specialized type of endothelial cells (ECs) that acquires hemogenic potential (Gritz and Hirschi, 2016). Importantly, HE cells exhibit distinct functional properties depending on their origin sites (Chen et al., 2011). HE cells in yolk sac give rise to erythroid-myeloid progenitors (EMPs) without lymphoid potential (Cumano et al., 1996). In contrast, aorta-gonad-mesonephros (AGM) HE cells develop into hematopoietic stem cells (HSCs) that are capable of reconstructing hematopoietic system in lethally irradiated recipients (Zovein et al., 2008). Nonetheless, whether HE cells are present in the placenta and if so, which type of cells placental HE cells can produce remain unknown.

Macrophages are innate immune cells residing in distinct organs, and have been shown to be generated from HE-derived EMPs and HSCs (Gomez Perdiguero et al., 2015; Ginhoux and Guilliams, 2016). In human placenta, macrophages, also known as Hofbauer cells (HBCs), are involved in placental angiogenesis

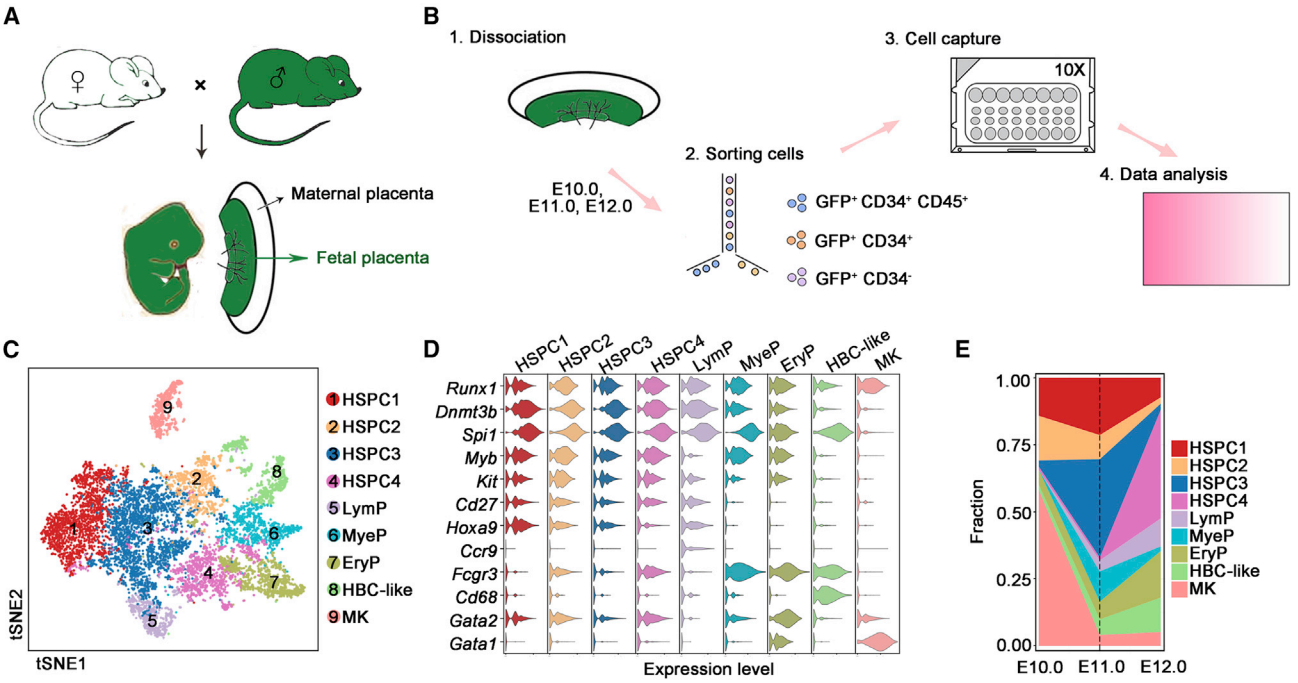

Figure 1. A single-cell-resolution transcriptomic atlas of mouse placenta

(A) Schematic representation of the cells of fetal origin in the mouse placenta.

(B) The illustration of mouse placenta scRNA-seq.

(C) Visualization of hematopoietic sub-clusters via *t*-distributed stochastic neighbor embedding (*t*-SNE).

(D) Violin plots showing the expression of selected feature genes in each cluster.

(E) The dynamical change of fraction of cell types at three developmental stages.

See also Figure S1 and Tables S2, S3, and S4.

and serve as a portal of entry of virus in placenta from viremic mothers (Zulu et al., 2019; Thomas et al., 2021). However, the origin of HBCs is still debated. Previous studies have shown that HBCs may directly arise from primitive macrophages and circulating monocytes (Selkov et al., 2013; Zulu et al., 2019; Thomas et al., 2021). Given that fate mapping in mouse model has illustrated origins of macrophages residing in many different tissues (Ginhoux and Guilliams, 2016), it seems plausible that the similar strategy could be employed to resolve the controversial origin of HBCs.

To address the aforementioned questions, we firstly employ single-cell RNA sequencing (scRNA-seq) to generate a cell atlas of mouse fetal placenta collected during the E10.0 to E12.0 period, when placental hematopoiesis occurs. Using this atlas, we identify the placental HE cells and characterize a placental EC-specific gene, *Hoxa13*. By generating a *Hoxa13* reporter line, we demonstrate that placenta serves as a hematopoietic organ for *de novo* generation of macrophages, named as HBC-like cells. Overall, the current study provides insights into placental hematopoiesis and further extends the potential clinical value of placenta as a new source of HE cells and macrophages.

RESULTS

A single-cell-resolution transcriptomic atlas of mouse placental hematopoiesis

Placenta has been demonstrated to be a hematopoietic organ during mammalian embryogenesis (Gekas et al., 2005; Alvarez-Silva et al., 2003). To explore the detailed developmental events of fetal hematopoiesis in mouse placenta, we first eliminated the contamination of maternal cells using the placentas resulting from the cross between EGFP$^+$ males and C57 BL/6 (EGFP$^-$) females, in which the fetal-derived cells are GFP positive (Alvarez-Silva et al., 2003). We then performed 10× Genomics-based scRNA-seq with GFP$^+$ cells to generate a fetal placental cell atlas (Figures 1A, 1B, and S1A; Table S2). In total, 16,205 cells from E10.0, E11.0, and E12.0 placenta passed stringent quality control, with a median of 4,100 genes per cell detected and retained for further analysis (Figure S1B). To annotate the major cell types in the developing placenta, Uniform Manifold Approximation and Projection (UMAP) analysis identified five major cell types based on differentially expressed genes (DEGs) between all clusters (Figures S1C–S1F; Tables S3 and S4) (Wolf et al., 2018). Hematopoietic cell types (Hema) were characterized by the expression of *Runx1*, *Kit*, and *Ptprc* (Figures S1C and S1D). As for the non-hematopoietic cell types, ECs (Endo) were identified by the expression of *Pecam1* and *Cdh5*, trophoblast cells (Trop) were identified by the expression of epithelial gene *Krt8*, stromal cells were identified by the expression of collagen genes *Col1a1* and *Col1a2*, and primitive endoderm (PrE) cells were identified by the expression of *S100g* (Figure S1E).

To characterize placental hematopoiesis in more details, hematopoietic cell clusters were further divided into nine distinct sub-clusters corresponding to six cell types (Figure 1C; Table S4). Among them, hematopoietic stem/progenitor cells (HSPCs)

express embryonic HSC markers *Cd34*, *Kit*, and *Cd27*; lymphoid progenitors (LymP) specifically express *Ccr9*; myeloid progenitors (MyeP) highly express *Spi1* and *Myb*; and HBC-like cells express *Cd68* (Figure 1D). Furthermore, to illustrate the dynamic changes in the abundance of these cell types in the placenta, we found that the fraction of hematopoietic cells changed dynamically, manifested as the increase in the fractions of HSPCs from E10.0 to E12.0 (Figure 1E). This finding agrees with the developmental hematopoiesis within the placenta (Gekas et al., 2005). Finally, we generated an interactive website (http://liulab.ioz.ac.cn/Placenta_hematopoiesis/), with all the data freely available to the community. Taken together, these findings reveal the cellular composition and cell-type-specific gene expression in the fetal placenta.

Identification of CD44$^+$ ECs with hemogenic potential in placenta

Since CD41$^+$ hematopoietic clusters had been observed in the placenta in the absence of circulation using *Ncx1* mutant mice (Rhodes et al., 2008), we wondered whether the cluster-forming HE cells exist in the placenta. To this end, all placental ECs were further divided into three sub-clusters, annotated as EC1, EC2, and EC3 (Figures 2A and 2B; Table S4). Among them, EC1 was characterized by the capillary feature with *Lyve1* expression (Gordon et al., 2008), EC2 showed the arterial feature with *Gja5* expression, and EC3 exhibited the venous feature with high expression of *Nr2f2* (Figure 2A). By analyzing the well-defined HE transcriptional features, such as Notch signaling (Hadland et al., 2015; Bigas et al., 2010), we found that EC2 highly expresses *Hey1*, *Hey2*, and *Jag1* (Figure 2C). In addition, *Prom1*, a placental hematopoietic potential marker (Pereira et al., 2016), was also specifically expressed in EC2 (Figure 2D). These results indicate that EC2 may be a specialized arterial EC, sharing similar transcriptional features with AGM-derived HE cells as previously reported (Gritz and Hirschi, 2016; Gao et al., 2018). To purify EC2 for further analysis, we characterized the immunophenotype of EC2 by examining the expression of candidate surface markers in three EC clusters (Figure 2D). Among them, *Cd44* was shown to be specifically expressed in EC2 but not in the other two clusters. Consistently, immunofluorescence (IF) analysis showed that CD44 staining was co-localized with a subset of CD31$^+$ ECs in E11.0 placenta (Figure 2E).

To further probe the hematopoietic output of EC2, the same number of CD44$^+$CD31$^+$CD45$^-$Ter119$^-$ cells (CD44$^+$ ECs) and CD44$^-$CD31$^+$CD45$^-$Ter119$^-$ cells (CD44$^-$ ECs) were captured by fluorescence-activated cell sorting (FACS), and then co-cultured with OP9-DL1 cells for 5 days (Figures S2A and S2B) (Li et al., 2013). Microscopic observation revealed that more round cells appeared in CD44$^+$ ECs, compared with CD44$^-$ ECs (Figure 2F). Moreover, quantitative PCR (qPCR) analysis showed that the expression of hematopoietic genes, *Runx1*, *Scl/Tal1*, and *Cmyb*, was upregulated, while the expression of endothelial gene *Flk1* was downregulated, indicating that CD44$^+$ ECs can be differentiated into hematopoietic cells (Figure 2G). Consistently, FACS analysis showed that higher proportion of CD34$^+$CD45$^+$c-Kit$^+$ cells occurred from CD44$^+$ ECs, compared with CD44$^-$ ECs (Figures 2H and S2C). To explore the hematopoietic properties of CD44$^+$ ECs-derived hematopoietic cells, colony-forming unit cell (CFU-C) assay showed that the number of hematopoietic colonies, including CFU-granulocyte-monocyte (CFU-GM) and CFU-mixed myeloid, megakaryocyte, and erythroid colonies (CFU-GEMM), was significantly higher than that from CD44$^-$ ECs (Figure 2I). As a control, we validated that both CD44$^+$ ECs and CD44$^-$ ECs do not generate hematopoietic colonies before co-culture with OP9-DL1 cells. Furthermore, to determine whether CD44 can label placenta ECs in humans, IF analysis showed that CD44 labeled a subset of human placental ECs at 9 weeks post conception (Figure S2D). Consistently, flow cytometry analysis demonstrated that 9.97% of human placental ECs were CD44 positive (Figure S2E). Additionally, UMAP analysis showed that the expression of *CD44* is restricted to fetal ECs but not maternal ECs in a previously published scRNA-seq dataset of human placenta (Figure S2F) (Vento-Tormo et al., 2018). Taken together, these data demonstrate that CD44 is expressed in a subset of ECs in both mouse and human placenta. More importantly, our functional studies indicate that CD44$^+$ ECs (named as "HE cells") can generate hematopoietic cells in the mouse placenta.

Comparison of placental and AGM HE cells

To compare the molecular features of HE cells in placenta and AGM, we first verified that CD44 can also be used to enrich HE cells in the AGM region (Figures S3A and S3B), consistent with a recent report (Oatley et al., 2020). Then we enriched HE cells and non-HE cells (CD44$^-$ ECs) from AGM and placenta at E11.0 and performed modified Smart-seq2 due to the rarity of HE cells (Figure S3C; Table S2). UMAP analysis showed that the HE and non-HE cells were clearly separated into two distinct sub-clusters. Moreover, HE and non-HE cells from placenta clustered more closely with each other than with their counterparts in AGM, suggesting that tissue environment could be a predominant factor affecting cell clustering (Figure 3A; Tables S3 and S5). Gene expression pattern showed that HE cells in AGM and placenta expressed several HE genes including *Prom1* and *Mecom* as well as high level of endothelial genes *Cdh5* and *Pecam1* (Figure 3B). To investigate the molecular cues in regulating HE cell formation, we identified DEGs between HE and non-HE cells in AGM and placenta and found that 58 genes were highly expressed both in AGM and placenta HE cells (Figure 3C; Table S5), including Notch-related genes *Hey1*, *Dll4*, and *Jag1* (Figure 3D). Interestingly, gene ontology (GO) analysis showed that "inflammatory response" is also enriched in HE cells of both sites, which agrees with the notion that proinflammatory signaling can instruct HE cells to generate HSPCs (Figure 3E; Table S5) (Gao et al., 2018; Mariani et al., 2019; He et al., 2015; Espín-Palazón et al., 2014; Sawamiphak et al., 2014).

To further investigate the tissue-specific transcriptomic features of HE cells, we compared placental and AGM HE cells. GO terms related to viral process are enriched in placental HE cells, in agreement with the presence of a blood-placenta barrier (Figure 3F; Table S5). Furthermore, to compare their hematopoietic properties *in vitro*, CFU-C assay showed that placental HE-derived hematopoietic cells exhibit higher colony-formation ability, with more GM and GEMM colonies, compared with AGM HE-derived cells (Figures 3G and 3H). Taken together, although HE cells in the placenta share the similar transcriptional

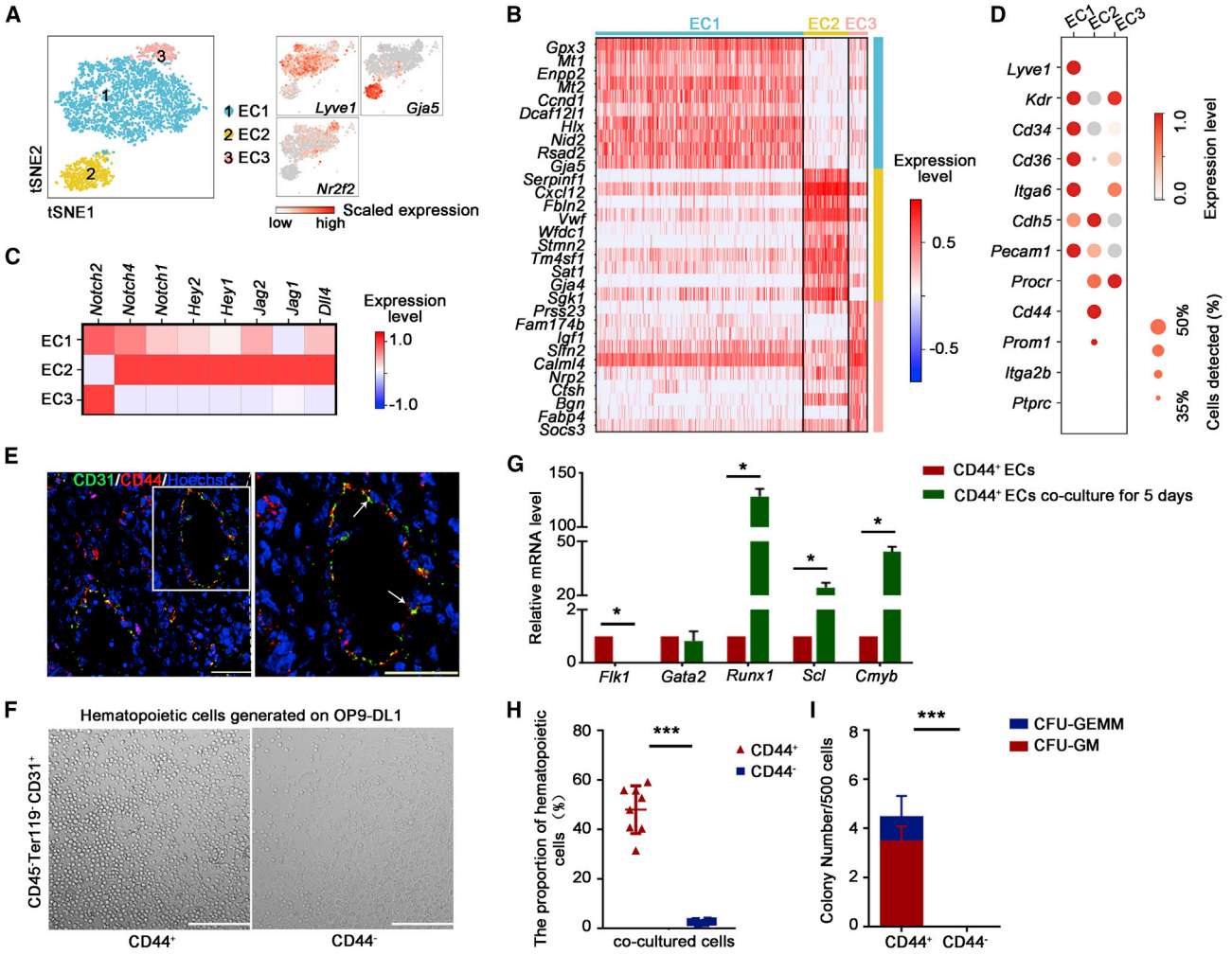

Figure 2. Identification of CD44$^+$ HE cells in placental ECs

(A) Visualization of endothelial sub-clusters in mouse fetal placenta by *t*-SNE (left). Cells are colored by their cell types. Feature plots displaying the expression of representative marker genes of defined cell groups (right).

(B) Heatmap showing the DEGs (top 10 genes) for three EC sub-clusters.

(C) Heatmap showing the expression of Notch-related genes in three EC sub-clusters.

(D) Dot plot showing the scaled expression level of surface markers in three EC sub-clusters.

(E) IF analysis of the mouse placenta showing the co-localization of CD31$^+$ ECs and CD44 staining at E11.0, double-positive cells are marked with white arrows. Data are from 3 independent experiments.

(F) Round hematopoietic cells generated from CD44$^+$ ECs (CD44$^+$CD31$^+$CD45$^-$Ter119$^-$) and CD44$^-$ ECs (CD44$^-$CD31$^+$CD45$^-$Ter119$^-$) after 5-day co-culture with OP9-DL1 cells.

(G) qPCR analysis showing the downregulation of *Flk1* and up-regulation of *Gata2*, *Runx1*, *Scl*, and *Cmyb* after 5-day co-culture. Number, n = 3.

(H) Statistical graph showing the proportion of generated hematopoietic cells from CD44$^+$ ECs and CD44$^-$ ECs. $n_{CD44+} = 8$; $n_{CD44-} = 6$.

(I) Colony-forming unit cell (CFU-C) assay of generated hematopoietic cells (CD45$^+$) from CD44$^+$ ECs and CD44$^-$ ECs, n = 3. Scale bars, 50 μm. Error bars, mean ± SD, *$p < 0.05$, ***$p < 0.001$.

See also Figure S2; Tables S4.

features with the AGM counterparts, they exhibit placenta-specific features, in terms of immunity and blood-placenta barrier and have higher hematopoietic abilities.

Generation of placental EC-specific *Hoxa13* transgenic mouse model

Given that there is no direct evidence as to whether placental ECs can generate hematopoietic cells *in vivo*, we set out to identify the specifically expressed genes in placental ECs. To this end, ECs from yolk sac were added for modified Smart-seq2 and *Hoxa13* is identified as a candidate placenta-specific gene consequently by UMAP (Figures S4A and S4B). Similar results were also validated by our 10x Genomics data and IF analysis (Figures S4C and S4D). Furthermore, we verified that the expression of *Hoxa13* is restricted to allantois and cannot be detected in blood progenitors from E8.5 (Pijuan-Sala et al., 2019), EMPs from E9.5 (Zhu et al., 2020) and hematopoietic cells from E10.0 to E12.0 (Figures S4E and S4F).

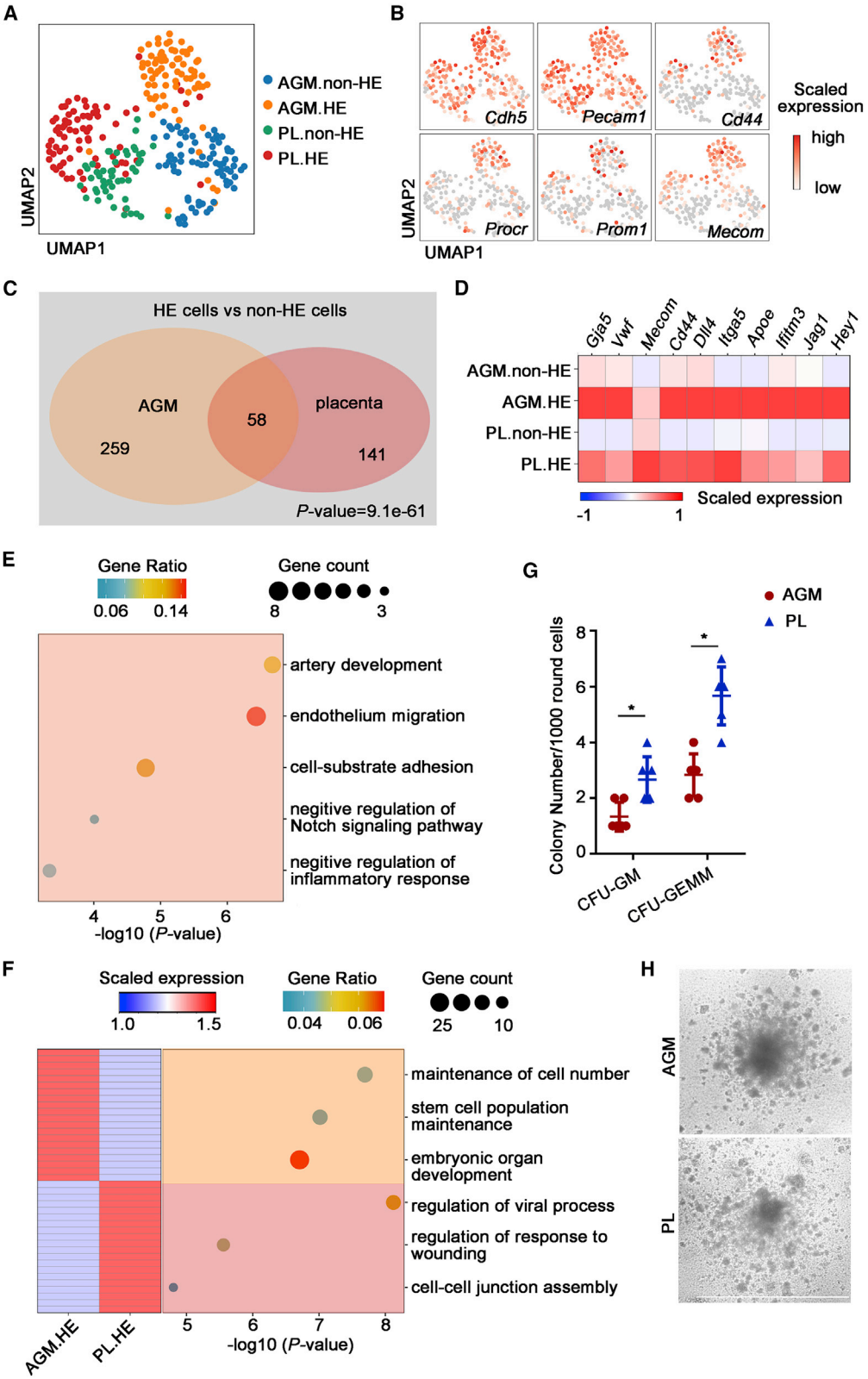

(legend on next page)

Based on the results above, we established a tamoxifen (TAM)-inducible model (named as *Hoxa13*^{CreER}) and crossed it with the *Rosa26*$^{mT/mG}$ reporter line (Figure 4A). In the *Hoxa13*^{CreER}; *Rosa26*$^{mT/mG}$ line, GFP fluorescence was used to label *Hoxa13*-expressing cells and their progenies after TAM injection. To eliminate the contamination of maternal cells, the placental cells were obtained from fetuses resulting from the cross between *Hoxa13*^{CreER} females and *Rosa*$^{mT/mG}$ males, in which the fetal component of placenta is tdTomato$^+$ or GFP$^+$ after TAM injection. First, *Hoxa13*$^+$ lineages were found in umbilical cord and placental vasculature, as well as in embryonic limbs at E11.0 when injecting TAM at E8.0, which is consistent with the role of Hoxa13 in embryonic limb development (Figures 4B–4D) (Stadler et al., 2001; Woltering et al., 2020). Moreover, IF analysis showed that *Hoxa13*$^+$ lineages are co-localized with ECs, and flow cytometry analysis showed that 39.1% ± 1.3% of CD31$^+$ ECs were GFP positive in the E11.0 placenta, supporting that *Hoxa13* labels a subset of placental ECs (Figures 4E, 4G, and 4H). In contrast, flow cytometry analysis showed that no GFP fluorescence was detected in *Hoxa13*^{CreER}; *Rosa26*$^{mT/mG}$ conceptus without TAM injection (Figure 4F). Furthermore, as expected, we validated that no GFP fluorescence can be detected in yolk sac and AGM ECs in *Hoxa13*^{CreER}; *Rosa26*$^{mT/mG}$ conceptus (Figures S4G–S4I). Taken together, these results suggest that *Hoxa13* is expressed in placental ECs and *Hoxa13*^{CreER} can be used to labeled placental ECs.

Hoxa13-mediated fate mapping reveals *de novo* generation of HBC-like cells from placental ECs

To interrogate the cell types of *Hoxa13*$^+$ lineages, flow cytometry analysis showed that 79.4% ± 2.1% of GFP$^+$ cells were CD31$^+$ ECs and 8.4% ± 1.0% of GFP$^+$ cells were CD45$^+$ hematopoietic cells in the E11.0 placenta (Figure S5A). To identify the cell types of *Hoxa13*$^+$ lineages at transcriptomic level, we sorted *Hoxa13*$^+$ lineages at E11.0, E12.0, and E13.5 placenta and performed modified Smart-seq2 (Figures S5A–S5C; Table S2). In total, 424 single cells passed rigorous quality control (Figures S5D and S5E; Table S3). To annotate the cell types, we performed UMAP and identified 4 cell types, including stromal cells, ECs, arterial ECs (AECs) and two clusters of HBC-like cells (Figure 5A; Table S6). Specifically, ECs were characterized by *Pecam1* expression, artery ECs (AECs) were characterized by *Gja5* expression and HBC-like cells were characterized by *Ptprc* and *Cd68* expression (Figure 5B).

To investigate the development path from placental ECs to hematopoietic cells, Monocle2 analysis predicated that the differentiation trajectory is from ECs toward AECs and finally produce HBC-like cells (Figure 5C). Different populations aligned along a pseudotime axis that followed the successive steps of the *in vivo* endothelial to hematopoietic (EHT). The concomitant loss of the endothelial program and initiation of the hematopoietic program were evidenced by the decreased expression of *Cdh5* and *Pecam1* and the increased expression of *Runx1*, *Kit*, and *Ptprc* (Figures 5D and 5E). Importantly, cells in the AEC expressed HE markers *Prom1*, *Procr*, and *Cd44* (Figure 5E), suggesting the existence of HE cells in AEC cluster. To investigate the function of *Hoxa13*$^+$ EC-derived HE cells, IF and flow cytometry analysis showed that *Hoxa13*$^+$ lineages were co-localized with CD44 staining and contributed to 34.8% ± 3.0% of HE cells in the E11.0 placenta (Figures 5F and S5F). Moreover, we co-cultured FACS-sorted GFP$^+$Ter119$^-$CD45$^-$CD31$^+$CD44$^+$ cells (named as GFP$^+$ HE cells) and GFP$^+$Ter119$^-$CD45$^-$CD31$^+$CD44$^-$ cells (named as GFP$^+$ non-HE cells) with OP9 cells, separately (Figure 5G). Microscopic observation revealed that after 7 days, the round cells were generated from GFP$^+$ HE cells, but not from GFP$^+$ non-HE cells. Additionally, flow cytometry analysis showed that a subset of these round cells is CD45 and CD68 double positive, suggesting that *Hoxa13*$^+$ EC-derived HE cells can generate HBC-like cells (Figures 5G and S5G). Taken together, these results demonstrate that *Hoxa13* labels a subset of placental HE cells that give rise to HBC-like cells.

To further examine the contribution of *Hoxa13*$^+$ lineages to HBC-like cells, flow cytometry analysis showed that 9.0% ± 1.9% of CD45$^+$CD68$^+$ HBC-like cells in the fetal placenta were GFP positive (Figure 5I). Additionally, to investigate the hematopoietic properties of GFP$^+$CD45$^+$ hematopoietic cells *in vitro*, CFU-C assay showed that these cells from the E13.5 placenta possess myeloid-biased differentiation potential (Figure 5J). Moreover, IF analysis also verified that *Hoxa13*$^+$ lineages overlap with CD68$^+$ HBC-like cells (Figure 5H). Moreover, we failed to detect *Hoxa13*$^+$ lineages in hematopoietic cells from yolk sac, AGM, and fetal liver (Figures S5H–S5J). These results indicate that placenta-derived hematopoietic cells exist exclusively in the placenta. Overall, these data represent a unique and reliable resource of placental hematopoiesis and demonstrate that a subset of HBC-like cells is derived from the *Hoxa13*$^+$ ECs in the placenta.

Characterization of two subtypes of *Hoxa13*$^+$ EC-derived HBC-like cells

To distinguish the two clusters of *Hoxa13*$^+$ EC-derived HBC-like cells (HBC-like-1 and -2), we examined the enrichment score of embryonic macrophage genes for *Hoxa13*$^+$ lineages (Zeng et al., 2019). The results indicate that gene signature of embryonic macrophages is highly enriched in HBC-like-1 and -2 (Figure S6A). Additionally, we characterized the immunophenotype

Figure 3. Comparison of placental and AGM HE cells

(A) UMAP visualization of HE cells and non-HE cells from placenta and AGM, respectively.
(B) Feature plots showing the expression of signature genes of HE cells and non-HE cells.
(C) Venn diagram showing the overlap of DEGs between HE cells and non-HE cells in AGM and placenta (Fisher's exact test p value = 9.1e−61).
(D) Heatmap showing the highly expressed genes in both HE cells of AGM and placenta.
(E) GO terms enriched in both HE cells of AGM and placenta.
(F) GO terms enriched in AGM and placental HE cells, respectively.
(G) CFU-C assay of generated hematopoietic cells from AGM and placental HE cells. n = 5.
(H) The morphology of colonies from generated hematopoietic cells. Scale bars, 50 μm. Error bars, mean ± SD, *p < 0.05.
See also Figure S3; Tables S2, S3, and S5.

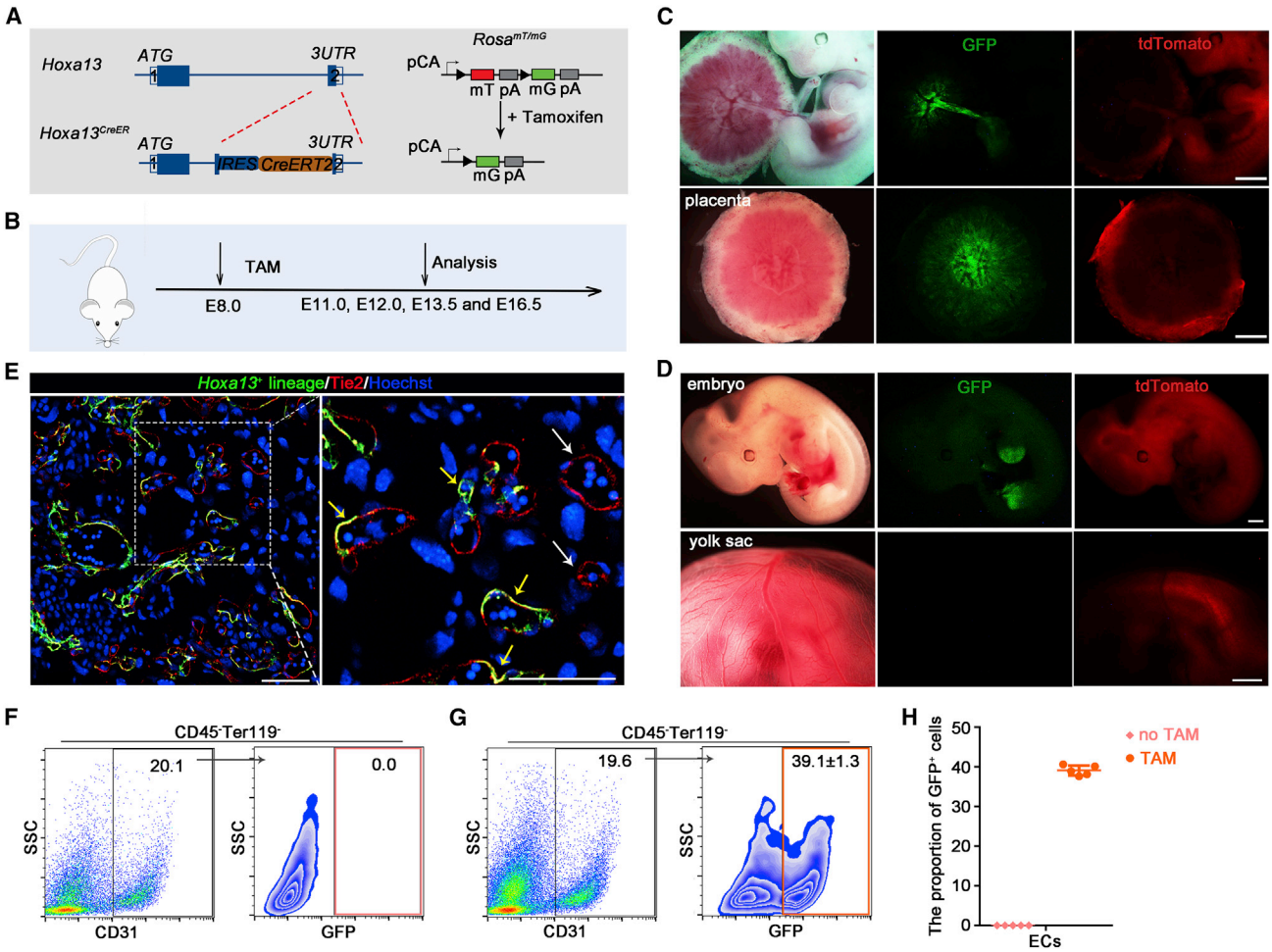

Figure 4. Generation of placental EC-specific *Hoxa13* transgenic mouse model

(A) Schematic diagram of *Hoxa13*^{CreER} mouse strategy. An *Ires-CreER* cassette was inserted into exon 2. *Hoxa13*^{CreER} mice were crossed with *Rosa26*$^{mT/mG}$ reporter mice.

(B) Experimental protocol. The pregnant mice were injected with tamoxifen (TAM) at E8.0, and the conceptuses were analyzed at different time points, including E11.0, E12.0, E13.5 and E16.5.

(C) Brightfield and fluorescence microscopy images in *Rosa*^{mTmG}; *Hoxa13*^{CreER} conceptus at E11.0 (top). GFP fluorescence detected in the placental vasculature and umbilical vessels (down), and tdTomato fluorescence detected in the conceptus.

(D) Brightfield and fluorescence microscopy images in *Rosa*^{mTmG}; *Hoxa13*^{CreER} embryo (top) and yolk sac (down) at E11.0. GFP fluorescence detected in the embryonic limbs, and tdTomato fluorescence detected in the embryo and yolk sac.

(E) IF analysis showing that a subset of ECs (Tie2$^+$) is co-localized with GFP at E11.0. Tie2$^+$ cells are marked with white arrows, and double-positive cells are marked with yellow arrows. Data are from 3 independent experiments.

(F) Flow cytometry analysis showing that no GFP$^+$ cells are detected in *Rosa*$^{mT/mG}$; *Hoxa13*^{CreER} placental ECs at E11.0 without TAM injection.

(G) Flow cytometry analysis showing that 39.1% ± 1.3% of ECs are GFP positive in *Rosa*$^{mT/mG}$; *Hoxa13*^{CreER} placenta at E11.0 after TAM injection.

(H) Statistical graph showing the proportion of GFP$^+$ ECs in the *Rosa*$^{mT/mG}$; *Hoxa13*^{CreER} placenta at E11.0 with and without TAM injection. n = 5. Scale bars, 50 μm.

See also Figure S4.

by examining the expression of candidate markers in these two clusters and found that *Cd74* was highly expressed in HBC-like-2 (Figure 6A). IF analysis validated the co-localization of *Hoxa13*$^+$ lineages and CD74$^+$ cells in placental labyrinth region (Figure 6B). To identify the 2 populations of HBC-like cells by flow cytometry, we defined CD45$^+$CD68$^+$CD74$^-$ cells as HBC-like-1, and CD45$^+$CD68$^+$CD74$^+$ cells as HBC-like-2 (Figure S6B). The morphology of HBC-like-1 and -2 was shown by Giemsa staining (Figure S6C). To quantify the proportion of GFP$^+$ cells in these two populations, flow cytometry analysis showed that in the E16.5 placenta, 7.1% ± 1.8% of HBC-like-1 were GFP positive and 9.5% ± 2.1% of HBC-like-2 were GFP positive (Figures 6C and S6B). Nevertheless, the proportion of GFP$^+$ cells between HBC-like-1 and -2 showed no significant difference (Figure 6C).

To further examine the role of HBC-like cells, 989 DEGs were identified between these two clusters. Among them, expression of 198 genes was upregulated and expression of 791 genes was downregulated in HBC-like-1, compared with HBC-like-2

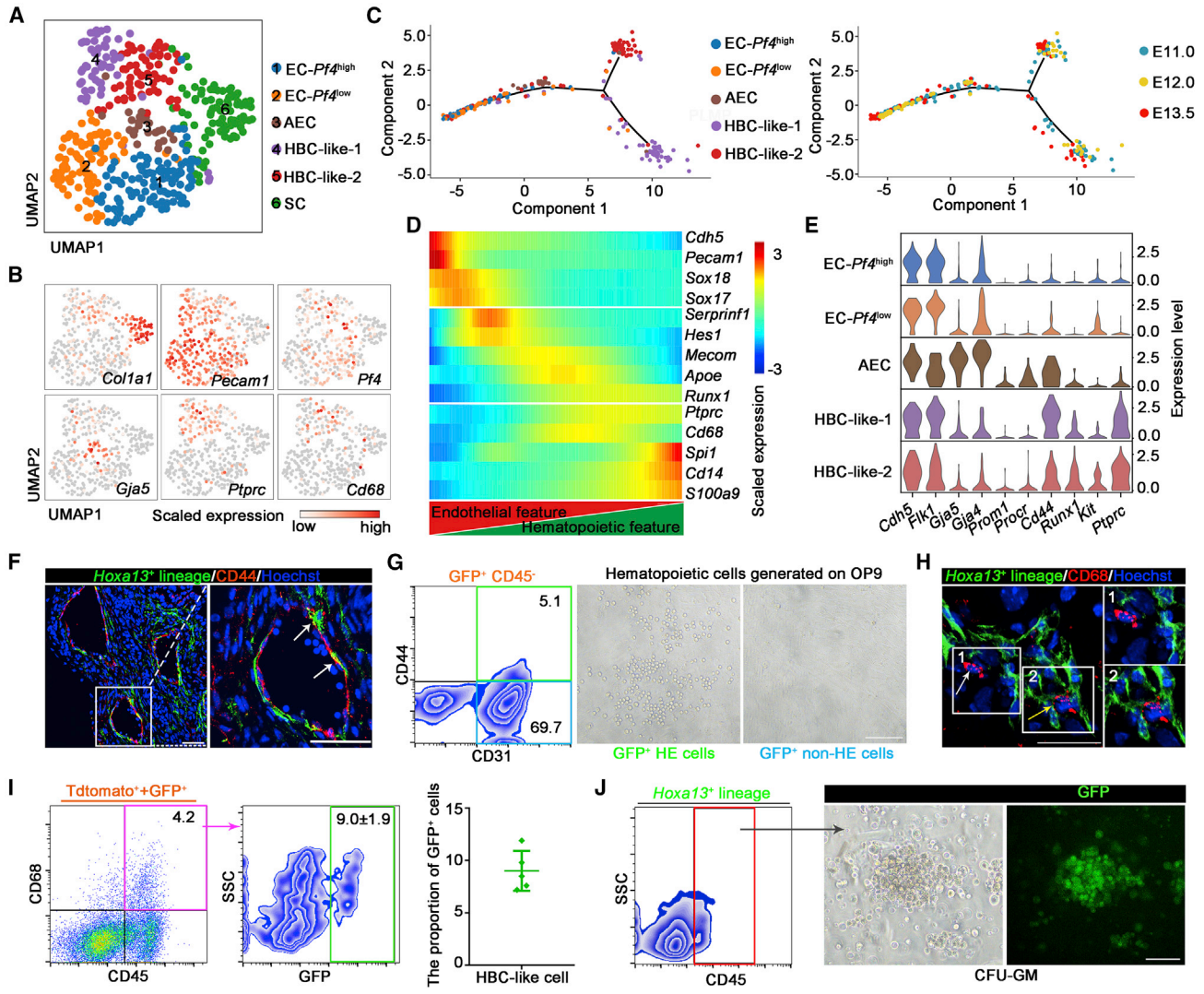

Figure 5. *Hoxa13*-mediated fate mapping reveals *de novo* generation of HBC-like cells from placental ECs

(A) UMAP visualization of *Hoxa13*$^{+}$ lineages from placenta.

(B) Feature plots showing the expression of signature genes of each cell type.

(C) Pseudotemporal ordering of cells in 5 selected clusters inferred by Monocle 2 with clusters (left) and the samples stages (right).

(D) Heatmap showing the dynamic expression of indicated genes from EC to HBC-like cell.

(E) Violin plots showing the expression of endothelial-to-hematopoietic (EHT) related genes in each cluster.

(F) IF analysis showing the co-localization of *Hoxa13*$^{+}$ lineage with CD44 staining, double-positive cells are marked with white arrows. Data are from 3 independent experiments.

(G) Representative FACS analysis of GFP^{+} HE (GFP^{+}CD31^{+}CD44^{+}CD45^{-}Ter119^{-}) cells and GFP^{+} non-HE cells (GFP^{+}CD31^{+}CD44^{-}CD45^{-}Ter119^{-}) in *Rosa*$^{mT/mG}$; *Hoxa13*^{CreER} placenta at E11.0 (left). Round hematopoietic cells generated from GFP^{+} HE cells after 7-day co-culture with OP9 cells (right).

(H) IF analysis showing the co-localization of *Hoxa13*$^{+}$ lineage with CD68 staining, double-positive cell is marked with yellow arrow. CD68^{+} cell is marked with white arrow.

(I) Representative flow cytometry analysis of total HBC-like cells in the fetal *Rosa*$^{mT/mG}$; *Hoxa13*^{CreER} placenta (CD45^{+} CD68^{+} [Tdtomato^{+}/GFP^{+}]) at E16.5 (left). Statistical graph showing the proportion of GFP^{+} HBC-like cells in CD68^{+} CD45^{+} population from fetal placenta GFP^{+} CD68^{+} CD45^{+} / (CD68^{+} CD45^{+} [tdTomato^{+} + GFP^{+}]) (right). n = 5.

(J) FACS analysis showing the hematopoietic cells (CD45^{+}) in *Hoxa13*$^{+}$ lineages in *Rosa*$^{mT/mG}$; *Hoxa13*^{CreER} placenta at E13.5 (left). CFU-C assay showing that GFP^{+} hematopoietic cells possess myeloid-biased hematopoietic potential *in vitro* (right). Scale bars, 50 μm. Error bars, mean ± SD.

See also Figure S5; Tables S2, S3, and S6.

(Figure 6D; Table S6). GO analysis of HBC-like-1 showed the enrichment of "inflammatory response" and "cytokine production" terms, evidenced by high expression of *Ccr1*, *Arg2*, *Lyz2*, and *Cxcr2*, suggesting its role in inflammation, consistent with that placentation is often considered as an inflammatory process in mammalian pregnancy (Figures 6E and 6F; Table S6) (Karakaya and Ozer, 2013; Chavan et al., 2016). Additionally, GO terms related to angiogenesis are also enriched in HBC-like-1,

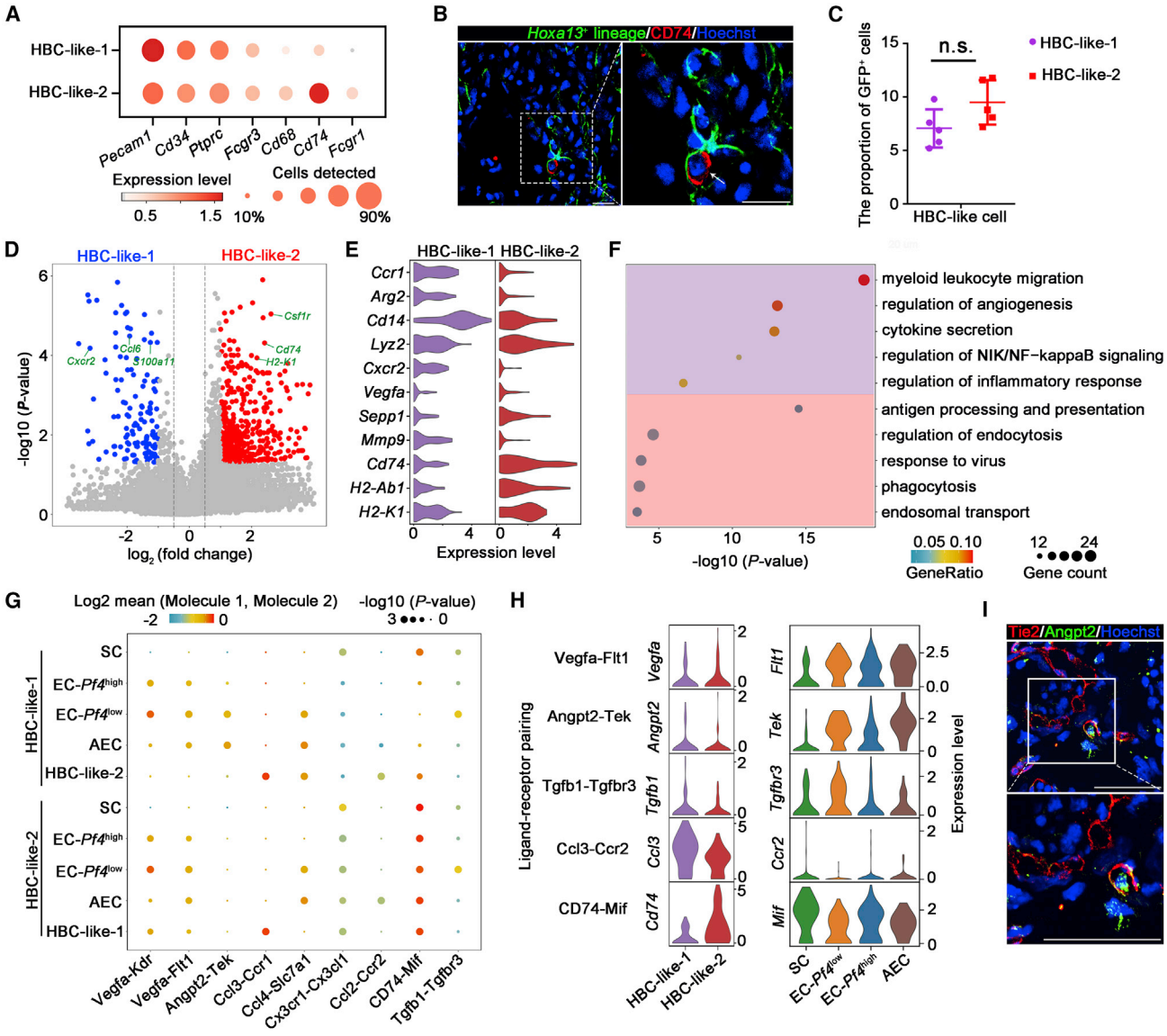

Figure 6. Characterization of two subtypes of *Hoxa13*$^+$ EC-derived HBC-like cells

(A) Dot plots showing the expression of surface markers in two HBC-like sub-clusters.

(B) IF analysis showing the co-localization of *Hoxa13*$^+$ lineage with CD74 staining, double-positive cell is marked with white arrow. Data are from 3 independent experiments.

(C) Statistical graph showing the proportion of GFP$^+$ cells in HBC-like-1 and -2, respectively. n = 5.

(D) Volcano plots of modified scRNA-seq data from HBC-like-1 and HBC-like-2. 198 genes are higher expressed in HBC-like-1and 791 genes are higher expressed in HBC-like-2.

(E) Violin plots showing the expression of signature genes in HBC-like-1 and HBC-like-2, respectively.

(F) GO terms enriched in HBC-like-1 (top) and -2 clusters (down).

(G) Overview of selected ligand-receptor interactions between HBC-like cells and other cell types.

(H) The expression of the ligand genes and its receptor genes of indicated pairings.

(I) IF analysis showing the spatial distribution between Tie2$^+$ ECs and Angpt2$^+$ cells in the placental labyrinth. Data are from 3 independent experiments. Scale bars, 50 μm. Error bars, mean ± SD, n.s., p ≥ 0.05.

See also Figure S6; Table S6.

which is evidenced by the high expression of *Vegfa*, *Sepp1*, and *Mpp9*, implying its potential pro-angiogenic function in placenta (Figures 6E and 6F; Table S6) (Plaks et al., 2013; Gerhardt et al., 2003; Ishikura et al., 2014). Moreover, GO analysis of HBC-like-2 showed the enrichment of "antigen processing and presentation" and "phagocytosis" terms, evidenced by high expression of *Cd74*, *H2-Ab1*, and *H2-K1*, consistent with the notion that placenta is a critical tissue barrier between maternal tissues and the fetus during pregnancy (Figures 6E and 6F; Table S6) (Zulu et al., 2019).

To analyze secretory and cell-surface molecules in HBC-like cells, we performed a computational framework, CellPhoneDB, to predict their interactions with other cells in the placenta (Vento-Tormo et al., 2018). Compared with HBC-like-2, HBC-like-1 expresses higher levels of *Vegfa*, whose receptor gene, *Flt1*, is expressed in ECs, suggesting a role of HBC-like-1 in regulating angiogenesis (Figures 6G and 6H). Moreover, the analysis also showed that HBC-like-1 interact with ECs via Angpt2-Tie2 signaling (Figures 6G and 6H), which has been shown to participate in angiogenesis during tumorigenesis (Han et al., 2016; Kapiainen et al., 2021), implying that HBC-like-secreted Angpt2 may play a potential role during placenta angiogenesis. We further performed IF to demonstrate the interaction of Tie2^{+} ECs and Angpt2^{+} cells in the placental labyrinth (Figure 6I). HBC-like-2 expresses higher levels of *Cd74*, whose ligand gene, *Mif*, is expressed in ECs and stromal cells, suggesting the role of HBC-like-2 in phagocytosis (Figures 6G and 6H) (Farr et al., 2020; Ives et al., 2021). Finally, to determine whether mouse and human placental macrophages are evolutionarily conserved, we thus compared our dataset with the recently published human placenta scRNA-seq dataset (Vento-Tormo et al., 2018; Thomas et al., 2021). UMAP visualization of integrated data indicated that HBC-like-1 and -2 merged well with HBC cluster in the human placenta (Figure S6D). Collectively, these results suggest that HBC-like cells play roles in inflammation, angiogenesis, and phagocytosis, which are evolutionarily conserved in human placental HBCs.

DISCUSSION

In this study, we performed scRNA-seq, combined with functional assay and fate mapping, to decode fetal placental hematopoiesis in mice. We profiled a single-cell atlas covering nearly all cell types of developing fetal placenta, with a focus on placental hematopoiesis. Importantly, we identified unique placental HE cells and established a new *Hoxa13*^{CreER} reporter line to trace placental EC and their derivatives. Finally, we identified that the HBC-like cells develop from *Hoxa13*$^{+}$ ECs and further to promote angiogenesis and phagocytosis. Overall, we revealed that placenta serves as a newly defined hematopoietic organ for macrophage *de novo* generation.

During mouse embryogenesis, HE cells can be identified in different anatomical locations including yolk sac and AGM (Gao et al., 2018). In this study, we identified HE cells in the mouse placenta by using a surface marker CD44 that can purify ECs with hemogenic potential as reported in mouse and human AGM region recently (Oatley et al., 2020; Zeng et al., 2019). In addition, we also verified the conserved expression of CD44 in human placental ECs. However, further investigations will be needed to determine whether CD44 is able to label human placental HE cells specifically. Previous studies indicated that activation of arterial program is required for HE cell specification in mouse AGM and for the generation of HE cells with lymphoid potential from human pluripotent stem cells (Slukvin and Uenishi, 2019; Park et al., 2018). Of note, our transcriptomic analysis of HE cells and non-HE cells in the placenta reveal the arterial feature of HE cells, similar to their counterparts in AGM, prompting us to apply placental HE cells for hematopoietic cell generation in clinic.

In humans, HBCs have been demonstrated as the only fetal immune cells found in the critical tissue barrier site between maternal tissues and the fetus (Thomas et al., 2021). Previous studies show that HBCs are transcriptionally similar to primitive macrophages that is consistent with their predicted primitive origins, however, the exact origin of HBCs is still debated. Here, HBC-like cells in our 10x Genomics datasets, which contain all fetal placental macrophages, were further divided into four subpopulations with different transcriptional profiles, named as HBC-like-1^{10x}, -2^{10x}, -3^{10x} and -4^{10x} (Figure S6D; Table S4). Integrated analysis of modified smart-seq2-GFP datasets (*Hoxa13*$^{+}$ lineages), which only include *Hoxa13*-derived macrophages, and 10x Genomics datasets shows that HBC-like-3^{10x} and -4^{10x} are transcriptionally similar to HBC-like-1 and -2, respectively (Figure S6E; Table S7). This result indicates that HBC-like-3^{10x} and -4^{10x} may be derived from placental *Hoxa13*$^{+}$ ECs. Moreover, integral analysis of HBC-like cells in 10x Genomics datasets and yolk-sac EMP scRNA-seq datasets reveals that HBC-like-1^{10x} is transcriptionally similar to yolk-sac EMP, suggesting that it may be derived from yolk-sac EMP (Figure S6F) (Zhu et al., 2020). Taken together, we reason that placental-ECs-derived HBC-like cells provide additional sources for placental macrophages, in addition to EMP-derived macrophages during pregnancy.

Previous studies show that HBCs in human placenta produce factors to respond to inflammatory stimulation and promote placental angiogenesis (Burton et al., 2009; Arany and Hill, 1998). We also profile HBC-like cells in mouse placenta at transcriptomic level and predicted their cytokine production and pro-angiogenic function, consistent with the function of HBCs in the human placenta (Burton et al., 2009; Arany and Hill, 1998; Thomas et al., 2021). Meanwhile, cell-cell interaction analysis suggest that placental HBC-like cells may secrete Vegfa, Sepp1, Mmp9, and Angpt2, which have pro-angiogenic property (Wang et al., 2007; Plaks et al., 2013; Ishikura et al., 2014; Gerhardt et al., 2003). In human placenta, stimulating the angiotensin pathway will increase the expression of proliferative/angiogenic factors and the low levels of Angpt2 is associated with placental insufficiency (Wang et al., 2007; Carr et al., 2016). Further studies are required to identify whether the placentation defects, such as labyrinth branching defect, abnormal artery/vein morphology, and small placenta, are ascribed to HBC-like cells deficiency.

In summary, our findings demonstrate that, in addition to AGM and yolk sac, placenta is another hematopoietic organ for *de novo* macrophage generation. We identify the presence of placental HE cells, the origin and the biological function of HBC-like cells. Importantly, this work will deepen our understanding on mouse placental hematopoiesis and further extend the clinical value of placenta as a new source of HE cells and macrophages.

Limitations of the study

Placental macrophages are the only fetal immune cell population within the stroma of healthy placenta during pregnancy. Identification of their origin and function is important for a deep understanding of the occurrence of fetal placental immune response. Although this study reveals the novel placental HE origin of placental macrophages, currently, it is not clear whether and

how macrophages derived from different origins can be identified and distinguished based on their signatures. To address this important limitation, labeling the different origins of macrophages once they are produced will be a key objective for further studies. Furthermore, while the findings of this study have predicted the potential biological function of placental macrophages, there is currently no experimental evidence of their *in vivo* or *in vitro* function. Investigating their function based on mouse model and cell culture will be critical avenues to explore.

STAR★METHODS

Detailed methods are provided in the online version of this paper and include the following:

- KEY RESOURCES TABLE
- RESOURCE AVAILABILITY
  - Lead contact
  - Materials availability
  - Data and code availability
- EXPERIMENTAL MODELS AND SUBJECT DETAILS
  - Experiment models and biological samples
- METHOD DETAILS
  - Immunofluorescence
  - Preparation of single cell suspensions
  - Flow cytometry analysis
  - Hematopoietic cell induction
  - CFU-C assay
  - Quantitative real-time PCR
  - Generation of *Hoxa13*^{creER} line
  - The route and dosage of Tamoxifen induction
  - 10× genomics single cells RNA sequencing data pre-processing
  - Modified smart-seq2 sequencing data pre-processing
  - Single cell RNA sequencing data processing
  - Quality control of single cell RNA sequencing data
  - Dimension reduction and clustering
  - DEGs identification
  - GO and KEGG enrichment analysis
  - Differentiation trajectory analysis
  - Cell-cell interaction network
  - Cell-type composition analysis
- QUANTIFICATION AND STATISTICAL ANALYSIS

SUPPLEMENTAL INFORMATION

Supplemental information can be found online at https://doi.org/10.1016/j.devcel.2021.06.005.

ACKNOWLEDGMENTS

We thank Fuchou Tang for critical reading of this manuscript. This work was supported by grants from the National Key Research and Development Program of China (2018YFA0800200, 2018YFA0801000, and 2016YFA0100500 to F.L., 2018YFC1004101 to H.W., and 2020YFA0804000 to J.-D.J.H.), the Strategic Priority Research Program of the Chinese Academy of Sciences, China (XDA16010207 to F.L.), and the National Natural Science Foundation of China (31830061, 81530004 and 31425016 to F. L., 31900664 to H. W., and 91749205, 92049302, 32088101 to J.-D.J.H.).

AUTHOR CONTRIBUTIONS

G.L. and F.L. designed the study. G.L. performed most of the experiments with the help from X.J., B.H., Y.Z., S.G., Z.K., and D.M.; C.Z. preformed the bioinformatics analysis under the guidance of J.-D.J.H.; X.J. performed smart-seq2 under the guidance of H.W.; F.W. designed the transgenic mouse model. B.G. interpreted the data and assisted with the manuscript. G.L. and F.L. wrote the manuscript, with contributions from all authors.

DECLARATION OF INTERESTS

The authors declare no competing interests.

Received: November 22, 2020
Revised: April 30, 2021
Accepted: June 8, 2021
Published: June 30, 2021

REFERENCES

Alvarez-Silva, M., Belo-Diabangouaya, P., Salaün, J., and Dieterlen-Lièvre, F. (2003). Mouse placenta is a major hematopoietic organ. Development *130*, 5437–5444.

Anders, S., Pyl, P.T., and Huber, W. (2015). HTSeq–a Python framework to work with high-throughput sequencing data. Bioinformatics *31*, 166–169.

Arany, E., and Hill, D.J. (1998). Fibroblast growth factor-2 and fibroblast growth factor receptor-1 mRNA expression and peptide localization in placentae from normal and diabetic pregnancies. Placenta *19*, 133–142.

Basu, S., Ray, A., and Dittel, B.N. (2013). Differential representation of B cell subsets in mixed bone marrow chimera mice due to expression of allelic variants of CD45 (CD45.1/CD45.2). J. Immunol. Methods *396*, 163–167.

Bigas, A., Robert-Moreno, A., and Espinosa, L. (2010). The Notch pathway in the developing hematopoietic system. Int. J. Dev. Biol. *54*, 1175–1188.

Burton, G.J., Woods, A.W., Jauniaux, E., and Kingdom, J.C. (2009). Rheological and physiological consequences of conversion of the maternal spiral arteries for uteroplacental blood flow during human pregnancy. Placenta *30*, 473–482.

Carr, D.J., David, A.L., Aitken, R.P., Milne, J.S., Borowicz, P.P., Wallace, J.M., and Redmer, D.A. (2016). Placental vascularity and markers of angiogenesis in relation to prenatal growth status in overnourished adolescent ewes. Placenta *46*, 79–86.

Chavan, A.R., Bhullar, B.A., and Wagner, G.P. (2016). What was the ancestral function of decidual stromal cells? A model for the evolution of eutherian pregnancy. Placenta *40*, 40–51.

Chen, M.J., Li, Y., De Obaldia, M.E., Yang, Q., Yzaguirre, A.D., Yamada-Inagawa, T., Vink, C.S., Bhandoola, A., Dzierzak, E., and Speck, N.A. (2011). Erythroid/myeloid progenitors and hematopoietic stem cells originate from distinct populations of endothelial cells. Cell Stem Cell *9*, 541–552.

Cumano, A., Dieterlen-Lievre, F., and Godin, I. (1996). Lymphoid potential, probed before circulation in mouse, is restricted to caudal intraembryonic splanchnopleura. Cell *86*, 907–916.

Dobin, A., Davis, C.A., Schlesinger, F., Drenkow, J., Zaleski, C., Jha, S., Batut, P., Chaisson, M., and Gingeras, T.R. (2013). STAR: ultrafast universal RNA-seq aligner. Bioinformatics *29*, 15–21.

Downs, K.M. (2002). Early placental ontogeny in the mouse. Placenta *23*, 116–131.

Efremova, M., Vento-Tormo, M., Teichmann, S.A., and Vento-Tormo, R. (2020). CellPhoneDB: inferring cell-cell communication from combined expression of multi-subunit ligand-receptor complexes. Nat Protoc *15*, 1484–1506. https://doi.org/10.1038/s41596-020-0292-x.

Espín-Palazón, R., Stachura, D.L., Campbell, C.A., García-Moreno, D., Del Cid, N., Kim, A.D., Candel, S., Meseguer, J., Mulero, V., and Traver, D. (2014). Proinflammatory signaling regulates hematopoietic stem cell emergence. Cell *159*, 1070–1085.

Ewels. (2016). MultiQC: summarize analysis results for multiple tools and samples in a single report. Bioinformatics *32*, 3047–3048. https://doi.org/10.1093/bioinformatics/btw354.

Fang, J.S., Gritz, E.C., Marcelo, K.L., and Hirschi, K.K. (2016). Isolation of murine embryonic hemogenic endothelial cells. J. Vis. Exp. *112*.

Farr, L., Ghosh, S., and Moonah, S. (2020). Role of MIF cytokine/CD74 receptor pathway in protecting against injury and promoting repair. Front. Immunol. *11*, 1273.

Gao, L., Tober, J., Gao, P., Chen, C., Tan, K., and Speck, N.A. (2018). RUNX1 and the endothelial origin of blood. Exp. Hematol. *68*, 2–9.

Gekas, C., Dieterlen-Lièvre, F., Orkin, S.H., and Mikkola, H.K. (2005). The placenta is a niche for hematopoietic stem cells. Dev. Cell *8*, 365–375.

Gekas, C., Rhodes, K.E., Van Handel, B., Chhabra, A., Ueno, M., and Mikkola, H.K. (2010). Hematopoietic stem cell development in the placenta. Int. J. Dev. Biol. *54*, 1089–1098.

Gerhardt, H., Golding, M., Fruttiger, M., Ruhrberg, C., Lundkvist, A., Abramsson, A., Jeltsch, M., Mitchell, C., Alitalo, K., Shima, D., and Betsholtz, C. (2003). VEGF guides angiogenic sprouting utilizing endothelial tip cell filopodia. J. Cell Biol. *161*, 1163–1177.

Ginhoux, F., and Guilliams, M. (2016). Tissue-resident macrophage ontogeny and homeostasis. Immunity *44*, 439–449.

Gomez Perdiguero, E., Klapproth, K., Schulz, C., Busch, K., Azzoni, E., Crozet, L., Garner, H., Trouillet, C., De Bruijn, M.F., Geissmann, F., and Rodewald, H.-R. (2015). Tissue-resident macrophages originate from yolk-sac-derived erythro-myeloid progenitors. Nature *518*, 547–551.

Gordon, E.J., Gale, N.W., and Harvey, N.L. (2008). Expression of the hyaluronan receptor LYVE-1 is not restricted to the lymphatic vasculature; LYVE-1 is also expressed on embryonic blood vessels. Dev. Dyn. *237*, 1901–1909.

Gritz, E., and Hirschi, K.K. (2016). Specification and function of hemogenic endothelium during embryogenesis. Cell. Mol. Life Sci. *73*, 1547–1567.

Gulati, G.S., Sikandar, S.S., Wesche, D.J., Manjunath, A., Bharadwaj, A., Berger, M.J., Ilagan, F., Kuo, A.H., Hsieh, R.W., Cai, S., et al. (2020). Single-cell transcriptional diversity is a hallmark of developmental potential. Science 367, 405–411. https://doi.org/10.1126/science.aax0249.

Hadland, B.K., Varnum-Finney, B., Poulos, M.G., Moon, R.T., Butler, J.M., Rafii, S., and Bernstein, I.D. (2015). Endothelium and NOTCH specify and amplify aorta-gonad-mesonephros-derived hematopoietic stem cells. J. Clin. Invest. *125*, 2032–2045.

Hamey, F.K., and Göttgens, B. (2019). Machine learning predicts putative hematopoietic stem cells within large single-cell transcriptomics data sets. Exp Hematol 78, 11–20. https://doi.org/10.1016/j.exphem.2019.08.009.

Han, S., Lee, S.J., Kim, K.E., Lee, H.S., Oh, N., Park, I., Ko, E., Oh, S.J., Lee, Y.S., Kim, D., et al. (2016). Amelioration of sepsis by TIE2 activation-induced vascular protection. Sci. Transl. Med. *8*, 335ra55.

He, Q., Zhang, C., Wang, L., Zhang, P., Ma, D., Lv, J., and Liu, F. (2015). Inflammatory signaling regulates hematopoietic stem and progenitor cell emergence in vertebrates. Blood *125*, 1098–1106.

Ishikura, K., Misu, H., Kumazaki, M., Takayama, H., Matsuzawa-Nagata, N., Tajima, N., Chikamoto, K., Lan, F., Ando, H., Ota, T., et al. (2014). Selenoprotein P as a diabetes-associated hepatokine that impairs angiogenesis by inducing VEGF resistance in vascular endothelial cells. Diabetologia *57*, 1968–1976.

Ives, A., Le Roy, D., Théroude, C., Bernhagen, J., Roger, T., and Calandra, T. (2021). Macrophage migration inhibitory factor promotes the migration of dendritic cells through CD74 and the activation of the Src/PI3K/myosin II pathway. FASEB J. *35*, e21418.

Kapiainen, E., Kihlström, M.K., Pietilä, R., Kaakinen, M., Ronkainen, V.P., Tu, H., Heikkinen, A., Devarajan, R., Miinalainen, I., Laitakari, A., et al. (2021). The amino-terminal oligomerization domain of angiopoietin-2 affects vascular remodeling, mammary gland tumor growth, and lung metastasis in mice. Cancer Res. *81*, 129–143.

Karakaya, Y.A., and Ozer, E. (2013). The role of Hofbauer cells on the pathogenesis of early pregnancy loss. Placenta *34*, 1211–1215.

Kechin, A., Boyarskikh, U., Kel, A., and Filipenko, M. (2017). cutPrimers: a new tool for accurate cutting of primers from reads of targeted next generation sequencing. J. Comput. Biol. *24*, 1138–1143.

Kim, D., Langmead, B., and Salzberg, S.L. (2015). HISAT: a fast spliced aligner with low memory requirements. Nat. Methods *12*, 357–360.

Koushik, S.V., Wang, J., Rogers, R., Moskophidis, D., Lambert, N.A., Creazzo, T.L., and Conway, S.J. (2001). Targeted inactivation of the sodium-calcium exchanger (Ncx1) results in the lack of a heartbeat and abnormal myofibrillar organization. FASEB J. *15*, 1209–1211.

Lee, L.K., Ueno, M., Van Handel, B., and Mikkola, H.K. (2010). Placenta as a newly identified source of hematopoietic stem cells. Curr. Opin. Hematol. *17*, 313–318.

Li, Z., Zhou, F., Chen, D., He, W., Ni, Y., Luo, L., and Liu, B. (2013). Generation of hematopoietic stem cells from purified embryonic endothelial cells by a simple and efficient strategy. J. Genet. Genomics *40*, 557–563.

Macosko, E.Z., Basu, A., Satija, R., Nemesh, J., Shekhar, K., Goldman, M., Tirosh, I., Bialas, A.R., Kamitaki, N., Martersteck, E.M., et al. (2015). Highly parallel genome-wide expression profiling of individual cells using nanoliter droplets. Cell *161*, 1202–1214.

Mariani, S.A., Li, Z., Rice, S., Krieg, C., Fragkogianni, S., Robinson, M., Vink, C.S., Pollard, J.W., and Dzierzak, E. (2019). Pro-inflammatory aorta-associated macrophages are involved in embryonic development of hematopoietic stem cells. Immunity *50*, 1439–1452.e5.

McKinney-Freeman, S., Cahan, P., Li, H., Lacadie, S.A., Huang, H.T., Curran, M., Loewer, S., Naveiras, O., Kathrein, K.L., Konantz, M., et al. (2012). The transcriptional landscape of hematopoietic stem cell ontogeny. Cell Stem Cell *11*, 701–714.

Muzumdar, M.D., Tasic, B., Miyamichi, K., Li, L., and Luo, L. (2007). A global double-fluorescent Cre reporter mouse. Genesis *45*, 593–605.

Oatley, M., Bölükbası, Ö.V., Svensson, V., Shvartsman, M., Ganter, K., Zirngibl, K., Pavlovich, P.V., Milchevskaya, V., Foteva, V., Natarajan, K.N., et al. (2020). Single-cell transcriptomics identifies CD44 as a marker and regulator of endothelial to haematopoietic transition. Nat. Commun. *11*, 586.

Ottersbach, K., and Dzierzak, E. (2005). The murine placenta contains hematopoietic stem cells within the vascular labyrinth region. Dev. Cell *8*, 377–387.

Park, M.A., Kumar, A., Jung, H.S., Uenishi, G., Moskvin, O.V., Thomson, J.A., and Slukvin, I.I. (2018). Activation of the arterial program drives development of definitive hemogenic endothelium with lymphoid potential. Cell Rep. *23*, 2467–2481.

Pereira, C.F., Chang, B., Gomes, A., Bernitz, J., Papatsenko, D., Niu, X., Swiers, G., Azzoni, E., De Bruijn, M.F., Schaniel, C., et al. (2016). Hematopoietic reprogramming in vitro informs in vivo identification of hemogenic precursors to definitive hematopoietic stem cells. Dev. Cell *36*, 525–539.

Pijuan-Sala, B., Griffiths, J.A., Guibentif, C., Hiscock, T.W., Jawaid, W., Calero-Nieto, F.J., Mulas, C., Ibarra-Soria, X., Tyser, R.C.V., Ho, D.L.L., et al. (2019). A single-cell molecular map of mouse gastrulation and early organogenesis. Nature *566*, 490–495.

Plaks, V., Rinkenberger, J., Dai, J., Flannery, M., Sund, M., Kanasaki, K., Ni, W., Kalluri, R., and Werb, Z. (2013). Matrix metalloproteinase-9 deficiency phenocopies features of preeclampsia and intrauterine growth restriction. Proc. Natl. Acad. Sci. USA *110*, 11109–11114.

Qiu, X., Mao, Q., Tang, Y., Wang, L., Chawla, R., Pliner, H.A., and Trapnell, C. (2017). Reversed graph embedding resolves complex single-cell trajectories. Nat. Methods *14*, 979–982.

Rhodes, K.E., Gekas, C., Wang, Y., Lux, C.T., Francis, C.S., Chan, D.N., Conway, S., Orkin, S.H., Yoder, M.C., and Mikkola, H.K. (2008). The emergence of hematopoietic stem cells is initiated in the placental vasculature in the absence of circulation. Cell Stem Cell *2*, 252–263.

Rossant, J., and Cross, J.C. (2001). Placental development: lessons from mouse mutants. Nat. Rev. Genet. *2*, 538–548.

Sánchez, M.J., Holmes, A., Miles, C., and Dzierzak, E. (1996). Characterization of the first definitive hematopoietic stem cells in the AGM and liver of the mouse embryo. Immunity *5*, 513–525.

Sawamiphak, S., Kontarakis, Z., and Stainier, D.Y. (2014). Interferon gamma signaling positively regulates hematopoietic stem cell emergence. Dev. Cell *31*, 640–653.

Shannon, P., Markiel, A., Ozier, O., Baliga, N.S., Wang, J.T., Ramage, D., Amin, N., Schwikowski, B., and Ideker, T. (2003). Cytoscape: a software environment for integrated models of biomolecular interaction networks. Genome Res 13, 2498–2504. https://doi.org/10.1101/gr.1239303.

Selkov, S.A., Selutin, A.V., Pavlova, O.M., Khromov-Borisov, N.N., and Pavlov, O.V. (2013). Comparative phenotypic characterization of human cord blood monocytes and placental macrophages at term. Placenta *34*, 836–839.

Slukvin, I.I., and Uenishi, G.I. (2019). Arterial identity of hemogenic endothelium: a key to unlock definitive hematopoietic commitment in human pluripotent stem cell cultures. Exp. Hematol. *71*, 3–12.

Stadler, H.S., Higgins, K.M., and Capecchi, M.R. (2001). Loss of Eph-receptor expression correlates with loss of cell adhesion and chondrogenic capacity in Hoxa13 mutant limbs. Development *128*, 4177–4188.

Stuart, T., Butler, A., Hoffman, P., Hafemeister, C., Papalexi, E., Mauck, W.M., 3rd, Hao, Y., Stoeckius, M., Smibert, P., and Satija, R. (2019). Comprehensive integration of single-cell data. Cell *177*, 1888–1902.e21. https://doi.org/10.1016/j.cell.2019.05.031.

Sugiyama, D., Joshi, A., Kulkeaw, K., Tan, K.S., Yokoo-Inoue, T., Mizuochi-Yanagi, C., Yasuda, K., Doi, A., Iino, T., Itoh, M., et al. (2017). A transcriptional switch point During hematopoietic stem and progenitor cell ontogeny. Stem Cells Dev. *26*, 314–327.

Thomas, J.R., Appios, A., Zhao, X., Dutkiewicz, R., Donde, M., Lee, C.Y.C., Naidu, P., Lee, C., Cerveira, J., Liu, B., et al. (2021). Phenotypic and functional characterization of first-trimester human placental macrophages, Hofbauer cells. J. Exp. Med. *218*, e20200891.

Vento-Tormo, R., Efremova, M., Botting, R.A., Turco, M.Y., Vento-Tormo, M., Meyer, K.B., Park, J.E., Stephenson, E., Polanski, K., Goncalves, A., et al. (2018). Single-cell reconstruction of the early maternal-fetal interface in humans. Nature *563*, 347–353.

Wang, Y., Tasevski, V., Wallace, E.M., Gallery, E.D., and Morris, J.M. (2007). Reduced maternal serum concentrations of angiopoietin-2 in the first trimester precede intrauterine growth restriction associated with placental insufficiency. BJOG *114*, 1427–1431.

Wolf, F.A., Angerer, P., and Theis, F.J. (2018). SCANPY: large-scale single-cell gene expression data analysis. Genome Biol. *19*, 15.

Woltering, J.M., Irisarri, I., Ericsson, R., Joss, J.M.P., Sordino, P., and Meyer, A. (2020). Sarcopterygian fin ontogeny elucidates the origin of hands with digits. Sci. Adv. *6*, eabc3510.

Yu, G., Wang, L.G., Han, Y., and He, Q.Y. (2012). clusterProfiler: an R package for comparing biological themes among gene clusters. Omics *16*, 284–287.

Zeng, Y., He, J., Bai, Z., Li, Z., Gong, Y., Liu, C., Ni, Y., Du, J., Ma, C., Bian, L., et al. (2019). Tracing the first hematopoietic stem cell generation in human embryo by single-cell RNA sequencing. Cell Res. *29*, 881–894.

Zhang, C., Zheng, Y., Li, X., Hu, X., Qi, F., and Luo, J. (2019). Genome-wide mutation profiling and related risk signature for prognosis of papillary renal cell carcinoma. Ann. Transl. Med. *7*, 427.

Zhu, Q., Gao, P., Tober, J., Bennett, L., Chen, C., Uzun, Y., Li, Y., Howell, E.D., Mumau, M., Yu, W., et al. (2020). Developmental trajectory of pre-hematopoietic stem cell formation from endothelium. Blood *136*, 845–856.

Zovein, A.C., Hofmann, J.J., Lynch, M., French, W.J., Turlo, K.A., Yang, Y., Becker, M.S., Zanetta, L., Dejana, E., Gasson, J.C., et al. (2008). Fate tracing reveals the endothelial origin of hematopoietic stem cells. Cell Stem Cell *3*, 625–636.

Zulu, M.Z., Martinez, F.O., Gordon, S., and Gray, C.M. (2019). The elusive role of placental macrophages: the Hofbauer cell. J. Innate Immun. *11*, 447–456.

STAR★METHODS

KEY RESOURCES TABLE

REAGENT or RESOURCE	SOURCE	IDENTIFIER
Antibodies		
FITC anti-mouse CD45.1	eBioscience	Cat# 11-0451-81
PE-Cyanine7 anti-mouse CD45.2	eBioscience	Cat# 25-0454-80
APC anti-mouse CD45.2	Biolegend	Cat# 109814
APC anti-mouse CD117	eBioscience	Cat# 17-1171-82
APC anti-mouse CD3e	eBioscience	Cat# 17-0031-81
PE anti-mouse B220	eBioscience	Cat# 12-0452-81
PE anti-mouse Gr1	eBioscience	Cat# 12-5931-81
APC anti-mouse CD11b	eBioscience	Cat# 17-0112-81
PE-Cyanine 7 anti-mouse Ter119	eBioscience	Cat# 25-5921-81
PE-Cyanine 5 anti-mouse Ter119	BioLegend	Cat# 116209
PE-Cyanine 7 anti-mouse CD31	eBioscience	Cat# 25-0311-82
Alexa Fluor 647 anti-mouse CD34	eBioscience	Cat# 152205
PE-Cyanine 5 anti-mouse CD45	BioLegend	Cat# 103109
APC-eFluor 780 anti-mouse CD45	eBioscience	Cat# 47-0451-82
PE anti-Human/Mouse CD44	eBioscience	Cat# 12-0441-81
Brilliant Violet 421 anti-mouse CD68	BioLegend	Cat# 137017
Alexa Fluor 647 anti-mouse CD74	BioLegend	Cat# 151004
7-AAD	BioLegend	Cat# 420404
Hoechst	Invitrogen	Cat# 33342
Rabbit monoclonal anti-Runx1	Abcam	Cat# ab92336
Rat monoclonal anti-CD31	Abcam	Cat# ab56299
Mouse monoclonal anti-CD34	ZSGB-BIO	Cat# TA808864
Mouse monoclonal anti-CD74	Santa Cruz	Cat# SC6262
Rabbit monoclonal anti-CD44	Abcam	Cat# ab157107
Rabbit monoclonal anti-Hoxa13	ABclonal	Cat# A9564
Goat polyclonal anti-Tie2	R&D	Cat# AF762
Rabbit polyclonal anti-Angiopoietin 2	Abcam1	Cat# ab8452
Rat monoclonal anti-CD68	Abcam1	Cat# ab53444
Rabbit monoclonal anti-CD14	Abcam1	Cat# ab221678
Alexa Fluor 488 goat anti-rabbit IgG (H+L)	Invitrogen	Cat# A-11034
Alexa Fluor 488 goat anti-mouse IgG (H+L)	Invitrogen	Cat# A-11001
Alexa Fluor 488 donkey anti-rat IgG (H+L)	Invitrogen	Cat# A-21208
Alexa Fluor 555 goat anti-mouse IgG (H+L)	Invitrogen	Cat# A-21422
Alexa Fluor 594 donkey anti-goat IgG (H+L)	Invitrogen	Cat# A-11058
Alexa Fluor 594 gat anti-rat IgG (H+L)	Invitrogen	Cat# A11007
Alexa Fluor 594 gat anti-rabbit IgG (H+L)	Invitrogen	Cat# A-11037
Alexa Fluor 647 goat anti-rat IgG (H+L)	Invitrogen	Cat# A-21247
Alexa Fluor 647 donkey anti-goat IgG (H+L)	Invitrogen	Cat# A-21447
Chemicals, Peptides, and Recombinant Proteins		
RNeasy Mini Kit	QIAGEN	Cat# 74104
RNAiMAX	Invitrogen	Cat# 13778030
DPBS	Gibco	Cat# 14190144
Fetal bovine serum	Gibco	Cat# 16000044
MEM α	Gibco	Cat# 12561056

(*Continued on next page*)

Continued

REAGENT or RESOURCE	SOURCE	IDENTIFIER
1X RBC lysis buffer	eBioscience	Cat# 00-4333-57
M3434	Stem Cell Technologies	Cat# 03434
M5300	Stem Cell Technologies	Cat# 5350
Tissue freezing medium (OCT)	Leica	Cat# 20108926
KAPA HiFi HotStart ReadyMix (2X)	KAPA Biosystems	Cat# KK2601
SuperScript II reverse transcriptase	Invitrogen	Cat# 18064-014
Fixation/Permeabilization Solution Kit	BD Cytofix/Cytoperm	Cat# 554714
Betaine solution	Sigma-Aldrich	Cat# B0300-1VL
RNase inhibitor	TOYOBO	Cat# SIN-201
Recombinant murine Flt3-Ligand	PeproTech	Cat# 250-31L
Recombinant murine SCF	PeproTech	Cat# 250-03
Recombinant murine TPO	PeproTech	Cat# 315-14
Critical Commercial Assays		
Moloney Murine Leukemia Virus (M-MLV) reverse transcript	Promega	Cat# 90694
Deposited Data		
scRNA-seq raw data	This study	GEO: GSE152903
Webserver	This study	http://liulab.ioz.ac.cn/Placenta_hematopoiesis/
Experimental Models: Cell Lines		
OP9	ATCC	Cat# CRL-2749
OP9-DL1	N/A	N/A
Experimental Models: Organisms/Strains		
Mouse: C57BL/6	SPF	N/A
Mouse: B6.SJL	SPF	N/A
Mouse: *Rosa*^{mTmG}	SPF	N/A
Mouse: *Hoxa13*^{CreER}	This paper	N/A
Oligonucleotides		
Primers for qPCR, see Table S1	This paper	N/A
Software and Algorithms		
GraphPad Prism 6	GraphPad Software	https://www.graphpad.com/
Adobe Illustrator CC 2015	Adobe	https://www.adobe.com/cn/
Adobe Photoshop CS5	Adobe	https://www.adobe.com/cn/
FlowJo vX.0.7	FlowJo	https://www.flowjo.com/
FastQC	N/A	https://github.com/s-andrews/FastQC
MultiQC	(Ewels, 2016)	https://multiqc.info/
Cell Ranger (version 2.2.0)	10x Genomics	https://support.10xgenomics.com/
R v3.6.0	R Development Core Team	https://www.r-project.org/
Rstudio	Rstudio	https://www.rstudio.com/
Cutadapt (version 1.18)	Kechin et al., 2017	https://github.com/marcelm/cutadapt
Hisat2 (version 2.2.0)	Kim et al., 2015	http://daehwankimlab.github.io/hisat2/
Htseq (version 0.11.2)	Anders et al., 2015	https://htseq.readthedocs.io/en/master/
Seurat v3.1.5	(Stuart, 2019)	https://satijalab.org/seurat/
Cellphonedb	(Efremova, 2020)	https://github.com/Teichlab/cellphonedb
hscScore	Hamey, 2019	https://github.com/fionahamey/hscScore
Drop-seq_tools-2.0.0	Macosko et al., 2015	http://mccarrolllab.com/dropseq
STAR aligner	Dobin et al., 2013	https://github.com/alexdobin/STAR

(*Continued on next page*)

Continued

REAGENT or RESOURCE	SOURCE	IDENTIFIER
SCANPY (Version 1.4.4)	Wolf et al., 2018	https://github.com/theislab/scanpy
CytoTRACE	Gulati, 2020	https://cytotrace.stanford.edu/
Monocle2 (v 2.14.0)	Qiu et al., 2017	https://bioconductor.org/packages/release/bioc/html/monocle.html
Cluster Profiler	Yu et al., 2012	https://bioconductor.org/packages/release/bioc/html/clusterProfiler.html
enrichplot R package	Zhang et al., 2019	https://bioconductor.org/packages/release/bioc/html/enrichplot.html
cytoscape	Shannon, 2003	https://cytoscape.org/

RESOURCE AVAILABILITY

Lead contact

Further information and requests for resources and reagents should be directed to and will be fulfilled by the Lead Contact, Feng Liu (liuf@ioz.ac.cn).

Materials availability

Mouse generated for this study is listed in the Key resources table and available from the lead contact.

Data and code availability

The scRNA-seq data reported in this paper have been deposited in the Gene Expression Omnibus (GEO) under accession number GSE152903. The transcriptional atlas can be explored at http://liulab.ioz.ac.cn/Placenta_hematopoiesis/. All other relevant data and code in this study are available from the corresponding authors upon reasonable request.

EXPERIMENTAL MODELS AND SUBJECT DETAILS

Experiment models and biological samples

Wide-type C57BL/6 mice (CD45.2 background) were purchased from SPF (Beijing) Biotechnology Co., Ltd. EGFP mice (gift from F. Gao, Institute of Zoology, Beijing, China) and *Rosa26*^{mTmG} Reporter mice (Gift from L. Li, Institute of Zoology, Beijing, China) were used as previously described (Basu et al., 2013, Muzumdar et al., 2007). The mice were used for timed mating, with the morning of detection of vaginal plug defining as E0.5. Placentas were dissected and separated from the maternal decidua and umbilical cord. For flow cytometry analysis and single cell RNA sequencing, male EGFP mice were crossed with C57BL/6 mice to obtain the fetal component of the placenta (hereafter designated as GFP$^+$ placenta) as previously described (Alvarez-Silva et al., 2003). Animal experiments and procedures were approved by the Ethical Review Committee in the Institute of Zoology, Chinese Academy of Sciences.

Human placental tissues were collected in accordance with the policy of the Ethics Committee of the Beijing Obstetrics and Gynecology Hospital. Informed consent was obtained from all women who donated their placentae. Samples were used according to standard experimental protocols approved by the Ethics Committee of the Institute of Zoology, Chinese Academy of Sciences. Placentas from the first trimester (8~9 weeks of gestation) were collected for the isolation of single cells or for immunofluorescence studies.

METHOD DETAILS

Immunofluorescence

For mice, immunofluorescence assay for embryos and placentae was performed as previous reported. WT and GFP$^+$ placentas were separated from maternal decidua and fixed in 1% paraformaldehyde (PFA)/PBS for 8-12 h at 4°C, followed by 30% sucrose/PBS solution overnight. Then they were embedded and frozen in 100% OCT. Frozen sections were made into 10 μm and were blocked in 5% BSA (0.3% Triton X-100) for 1h at room temperature followed by incubated with primary antibodies (see Key resources table) overnight at 4°C diluted in 1% BSA. After rinsing, slides were incubated with secondary antibody specific to Rat, Rabbit, Goat, or Mouse based on the resource of primary antibody for 1 h at room temperature, and Hoechst was used to stain nucleus. Immunofluorescent images were acquired by a confocal laser microscope (A1; Nikon) and 3D projections were generated using Nikon confocal software.

For human placental tissues, the freshly collected human placenta of 9 weeks without decidua was immediately fixed in 4% paraformaldehyde overnight at 4°C, and then dehydrated and embedded in paraffin for histological sectioning. Paraffin sections were made into 5 μm and then dewaxed and rehydrated in xylene and ethanol gradients. Antigen epitopes were retrieved with citrate buffer by microwave heating (92–98 °C for 15 minutes). After cooling to room temperature, the sections were blocked with 5% BSA (0.3%

Triton X-100) for 1 hour at room temperature followed by incubation with primary antibodies (CD34, #TA808864, ZSGB-BIO; CD44, #ab157107, Abcam) overnight at 4°C diluted in 1% BSA. After rinsing, slides were incubated with species-specific secondary antibodies based on the source of primary antibodies for 1 hour at room temperature, and Hoechst was used to stain nuclei. Immunofluorescent images were acquired by a confocal laser microscope (A1; Nikon).

Preparation of single cell suspensions

For mice, placentas of pregnant mice were dissected and separated the maternal decidua and umbilical cord. Tissues were washed in PBS twice on ice and transferred to pre-warmed digestion medium containing 0.1 g/mL collagenase (Sigma) and 100 ug/mL DNase I (Sigma), followed by passed through 20G and 25G needles. Tissues were shaken for 30s and further incubated at 37°C for 30 min with general shaking every 5 minutes. Then tissues were centrifuged and washed in PBS, and transferred to cell dissociation reagent (Gibco) for 6-8 min at 37°C. Cell suspensions passed through 70 μm cell strainers (BD Falcon). Mouse AGM region was dissociated into single-cell suspensions as previously described(Fang et al., 2016).

For human placental tissues, the freshly collected human placenta of 9 weeks of gestation without decidua was placed in a Petri dish and was rinsed several times with PBS until no obvious blood clots observed. Then placental villi were scraped from the chorionic membrane using a scalpel, and the stripped membrane was discarded. The resultant placental villi were minced into small pieces with a scissor, and were then digested in an enzyme cocktail, which contains 0.125% trypsin (T4799, Sigma-Aldrich), 0.05% type IV collagenase (C5138, Sigma-Aldrich), 0.02% EDTA and 0.04% DNase (DN25, Sigma-Aldrich) in Dulbecco's modified eagle medium (DMEM, SH30243.01, HyClone), at 37 °C for 10 minutes in a shaking incubator with 100 revolutions per minute. The disaggregated cell suspension was passed through a 40-μm sterile cell strainer (352340, BD) and washed thoroughly with DMEM containing 10% FBS (10099-141, Gibco). Cells were pelleted from the filtrate by centrifugation and resuspended in DMEM containing 10% FBS. The undigested gelatinous tissue remnant was retrieved from the cell strainer and further digested in the enzyme cocktail with gentle shaking for another 10 minutes at 37 °C. The cells were then filtrated and pelleted as described before. Cells obtained from both enzyme digests were pooled together and passed through a 40-μm cell strainer. To exclude any remaining red blood cells, the filtrated cells were lysed with the red blood cell lysis buffer (00-4333-57, eBioscience). Finally, the pelleted placental cells were resuspended in DMEM containing 2% FBS for further flow cytometry analysis.

Flow cytometry analysis

Cells were stained with in FACS buffer (1 × PBS with 2% FBS) with specific surface antibodies (see Key resources table) for 30 min at 4 °C. Live cells were separated with 7-AAD. For intracellular antibody, cells were fixed using Fixation/Permeabilization Solution Kit for 30min at 4 °C, and then stained with specific antibodies. Cells were analyzed and sorted by MoFlo XDP (Beckman Coulter) and BD FACS Aria Fusion. Data were further analyzed with FlowJo software.

Hematopoietic cell induction

The OP9-DL1 cells were cultured in a 24-well plate for 1 day before co-culture, as previous described. Placentas were dissociated into single-cell suspensions before flow cytometry sorting. After antibody staining, 200 sorted $CD44^+$ ECs ($CD44^+CD31^+CD45^-Ter119^-$) and $CD44^-$ ECs ($CD44^-CD31^+CD45^-Ter119^-$) were co-cultured on OP9-DL1 stromal cells with culture medium α-MEM (Gibco), 10% FBS (Gibco), and cytokines (100ng/mL SCF, 100ng/mL Flt3 and 100ng/mL Flt3, all from PeproTech). After 5 days, co-cultured cells were collected for further analysis. For the hematopoietic production of *Hoxa13*-derived HE cells, OP9 cells were cultured in a 24-well plate for 1 day before co-culture. And FACS-sorted 200 GFP^+ HE cells ($CD44^+CD31^+CD45^-Ter119^-$) and 200 GFP^+ non-HE cells ($CD44^-CD31^+CD45^-Ter119^-$) were co-cultured on OP9 cells with culture medium as above mentioned. After 7 days, co-cultured cells were collected for further analysis.

CFU-C assay

For HE potential experiments, the $CD45^+$ hematopoietic cells from $CD44^+$ ECs or $CD44^-$ ECs co-cultured with OP9-DL1 stromal cells were harvested and added into MethoCult GF M3434 medium (Stem Cell Technologies) in ultra-low attachment 24-well plates (Costar). After cultured for 7-10 days at 37°C in 5% CO_2, the number of colonies including BFU-E, CFU-GM and CFU-GEMM was counted respectively. For the hematopoietic function of *Hoxa13*$^+$ lineages, the GFP^+ $CD45^+$ cells were harvested and performed CFU-C assay as above mentioned.

Quantitative real-time PCR

Total RNA of sorted cells was extracted by QIAGEN RNeasy Mini Kit (Cat. No. 74G4) and then reversed transcribed by oligo-dT to obtain cDNA as qPCR templates. The qPCR assays were performed with Bio-Rad system, and the expression of *Gapdh* for mouse was used as the internal control. The sequences of the qPCR primers used were listed in Table S1.

Generation of *Hoxa13*^{creER} line

gRNAs were designed using the CRISPR guide-design tool web (https://crispr.dbcls.jp/). The selected gRNA sequence is CCACGA CAAACCTCTC-TGAGAGG. The cassette of P2A-CreERT2-WPRE-SV40pA was designed for insertion at this gRNA position after CCACG. The targeting vector was constructed with 907 bp 5'arm and 1171 bp 3'arm. Mouse zygotes obtained by mating of males with super-ovulated C57BL/6 females were injected with a mixture of Cas9 mRNA (80 ng/μL), sgRNA (40 ng/μL) and donor vector

(10 ng/μL). Microinjections were performed into the male pronucleus of fertilized oocytes. Injected zygotes were transferred into pseudo-pregnant CD1 female mice, and viable adult mice were obtained. The correctly targeted mice were determined by PCR and sequencing analyses.

The route and dosage of Tamoxifen induction

For the tamoxifen induction, pregnant females were injected intraperitoneally with tamoxifen (100 mg/kg, Sigma-Aldrich #T-5648) dissolved in corn oil, along with progesterone (37.5 mg/kg, Sigma-Aldrich #P0130) subcutaneously at E8.0. An additional progesterone injection was given at E12.0 to help maintain pregnancy.

10× genomics single cells RNA sequencing data pre-processing

Placental cells were obtained from fetuses resulting from the cross between $EGFP^+$ males and C57BL/6 ($EGFP^-$) females, in which only the fetal-derived cells are GFP positive. GFP^+ placental cells of E10.0, E11.0 and E12.0 were prepared for single cell suspensions as above mention (Gekas et al., 2005). For placentae of E10.0 [30-34 somite pairs (sp)] and E11.0 (40-44 sp), 80,000 $CD34^+$ cells were isolated by FACS and pooled together with 20,000 $CD34^-$ cells at a ratio of 4:1 to enrich hematopoietic and endothelial cells (Sánchez et al., 1996, Sugiyama et al., 2017). For placentae of E12.0 (48-52 sp), about 20,000 $CD34^+$ $CD45^+$ hematopoietic progenitors (McKinney-Freeman et al., 2012), 20,000 $CD34^+$ cells and 10,000 $CD34^-$ cells were separately isolated, and then pooled together with $CD34^-$ cells at a ratio of 2:2:1 to enrich hematopoietic progenitors, hematopoietic and endothelial cells, respectively. (Table S2). Then single-cell suspensions were loaded on a Chromium Single Cell Controller (10× Genomics) to generate single-cell gel beads in emulsion (GEMs) by using Single Cell 30 Library and Gel Bead Kit V2 (10× Genomics, 120237) (CapitalBio Technology Corporation). RNAs barcoding were obtained through reverse transcription in individual GEMs. Barcoded cDNAs were pooled and cleaned up using beads (Invitrogen, 37002D). Single-cell RNA-sequencing (scRNA-seq) libraries were prepared using Single Cell 30 Library Gel Bead Kit V2 (10× Genomics, 120237) following the manufacture's introduction. Sequencing was performed on an Illumina HiSeq × Ten with pair end 150 bp (PE150).

Modified smart-seq2 sequencing data pre-processing

For modified smart-seq2 data, mouse yolk sac, AGM and placenta at E11.0 were dissected and prepared for single cell suspensions as above mention. Single cell suspensions were stained with Ter119, CD45, CD41, CD31, CD44 and 7AAD. Living HE cells ($CD44^+$ $CD31^+CD45^-Ter119^-$), non-HE cells ($CD44^-CD31^+CD45^-Ter119^-$) and ECs ($CD31^+CD45^-Ter119^-$) were isolated by FACS into individual wells of a 96-well plate containing 2.5 μl cell lysis buffer which was pipetted first (Table S2). For smart-seq2-GFP data, *Hoxa13*$^+$ lineages were obtained from the *Rosa26*^{mTmG}; *Hoxa13*^{CreER} placentas at E11.0, E12.0 and E13.5, were dissected and prepared for single cell suspensions, respectively. GFP^+ single cell isolated by FACS into individual wells of a 96-well plate containing 2.5 μl cell lysis buffer (Table S2). The cells were stored at -80 °C for later processing.

We further used a modified smart-seq2 protocol to construct the single-cell RNA-seq library. In short, the cells were lysed for releasing all RNAs; then the mRNAs were captured with barcoded oligo-dT primers with an anchor sequence and unique molecular identifier (UMI) sequences. The mRNAs were reverse-transcribed to the first-strand cDNAs. Then pre-amplification step was performed for increasing cDNA yields. Finally, cDNAs from different cells were pooled together with different barcodes. After 5 cycles of PCR, the index sequence with biotin modification was added at the 3' ends of the cDNAs. Following DNA fragmentation with ultrasonic apparatus, we used Dynabeads C1 (65002, Invitrogen) to enrich the 3' cDNAs to construct the library using a Kapa Hyper Prep Kit (KK8505, Kapa Biosystems). The pooled library was further amplified, subsequently purified twice with Ampure XP beads (Beckman). The cleaned libraries were then sent to the company of Novogene to do quality control and sequencing. The qualified libraries were sequenced by the Illumina Hiseq4000 platform with PE150 (paired end 150 bp reads) strategy.

Single cell RNA sequencing data processing

Raw data files from 3 samples based on 10×Genomics were processed by Cell Ranger software suite (version 2.2.0) with default mapping parameters, using the mm10 reference genome (Cell ranger reference version 1.2.0). Cellranger aggr was used to aggregate three cell ranger count runs together to remove batch effect.

For modified smart-seq2 dataset, read 2 grouped by barcodes was aligned to corresponding read 1 after removing ploy(A) and TSO sequence. Cutadapt (version 1.18) (Kechin et al., 2017) was used to remove the reads with low quality bases and adaptor contaminants. Clean reads were then aligned to mm10 reference genome (Ensemble) by Hisat2 (version 2.2.0) (Kim et al., 2015). Htseq (version 0.11.2) (Anders et al., 2015) was used to count uniquely mapped reads by the number of UMI sequence, finally produced the deduplicated genes expression matrix for the downstream analysis. For modified smart-seq2-GFP dataset, raw data were processed using the standard pipeline of Drop-seq_tools-2.0.0 (Macosko et al., 2015) and aligned by STAR aligner (Dobin et al., 2013) to the mm10 genome, which was incorporated with eGFP DNA sequence. The mapped reads were then tagged with GRCh38.84 annotation file, which was also incorporated with eGFP annotation information. Gene expression matrix (count value) of each cell was finally generated with the Digital Expression command.

Quality control of single cell RNA sequencing data

For 10×Genomics sequencing data, 16,205 cells whose detected gene number is more than 800 and less than 7000 were retained after filtered by mitochondrial gene percentage less than 0.09 (Table S3). For modified smart-seq2 sequencing dataset, we retained

cell with more than 1000 and less than 5000 detected genes, removing those with mitochondrial gene percentage more than 0.1 (Table S3). For modified smart-seq2-GFP dataset, cells with more than 200 less than 6000 genes and 0.2 mitochondrial gene percentage were retained (Table S3).

Dimension reduction and clustering

Single-Cell Analysis in Python (SCANPY) toolkit (Version 1.4.4) (Wolf et al., 2018) was used for dimension reduction and other downstream analysis. In brief, total count matrix was normalized by library-size correction using default size factor 10,000. Highly variable genes (HVGs) were calculated by function pp.highly_variable_genes with default parameters. Finally, 2024, 3439 and 3359 HVGs were identified as input to perform PCA analysis in 10× Genomics, modified smart-seq2 and modified smart-seq-2-GFP sequencing data respectively. For 10× Genomics data, after computing neighborhood graph (n_neighbor=20) using the top 50 principal components (PCs), Uniform Manifold Approximation and Projection (UMAP) was used to project cells into 2 dimensions, Louvain algorithm was used with parameter "resolution" = 0.9 to identify the cell clusters. We annotated the clusters into 5 cell types based on the known marker genes and then Hema and Endo clusters were shown by *t*-distributed stochastic neighbor embedding (*t*-SNE) using 30 and 20 PCs (perplexity=40) respectively. HBC-like clusters were further identified by re performing reduction analysis based on top 50 PCs with n_neighbors=15. For modified smart-seq2 and modified smart-seq2-GFP data analysis, UMAP with 10 nearest neighbors, top 15 and 40 PCs were used for dimension reduction. Louvain with resolution 0.9 was used for modified smart-seq2-GFP data analysis and batch balanced k nearest neighbours (BBKNN) algorithm was used to combine datasets in each timepoint.

Single-cell Mac enrichment score were calculated by function sc.tl.score_genes in SCNAPY. Related CS10 macrophage data were downloaded from GSE135202 and same procedures was used to process dimension reduction and clustering analysis as describe above. The identification of top 50 significant genes in macrophage clusters were used as gene signature.

DEGs identification

To find differential expressing genes (DEGs) among each cell cluster, we used function sc.tl.rank_genes_groups in SCANPY to do Wilcoxon rank-sum test. Default parameters were used and genes with *p-value* < 0.05 were thought as significant differential expressing genes to show on heatmap plots (Tables S4, S5, and S6).

GO and KEGG enrichment analysis

Go term and KEGG pathway enrichment were analyzed by R package cluster Profiler (Yu et al., 2012) with simplify function to reduce redundant GO terms which has similarity higher than cutoff (cutoff=0.7). Top enriched GO terms (p value < 0.05) were visualized by enrichplot R package (Zhang et al., 2019) (Tables S4, S5, and S6).

Differentiation trajectory analysis

Monocle2 (v 2.14.0) (Qiu et al., 2017) was used to construct pseudotime trajectory on selected cell populations. The top 1100 DEGs (*q*-value < 0.01) were selected as ordering genes to sort cells into pseudo-time order. The Discriminative Dimensionality Reduction with Trees (DDRtree) method was applied to reduce data and construct the consequent development paths. The selected genes with smoothed scaled expression were plotted using function plot_pseudotime_heatmap.

Cell-cell interaction network

To calculate significant ligands, receptors and their interaction pairs among different clusters, cell-cell communication was predicted by Cellphonedb software (version 2.0, https://www.cellphonedb.org/) (Vento-Tormo et al., 2018). Default parameters were used for Cellphonedb except for threshold=0.1 to filter those cells expressed too low specific ligand or receptor genes. Genes were transformed into human symbol by Ensemble.

Cell-type composition analysis

For placental macrophage clusters, cross-species comparison was calculated with HBC cluster in human placental scRNA-seq data and HBC-like cells in modified smart-seq2-GFP data. Integration methods, including function scanpy.tl.ingest and harmony, were used after gene expression matrix was transformed into corresponding human symbol by Ensemble. Comparison of cell type similarity was calculated with HBC-like clusters in 10×Genomics data and yolk sac EMP scRNA-seq data. Similarity was calculated by Pearson correlation and hierarchically clustered was used function sc.tl.dengrogram in SCANPY (Table S7). The human placental scRNA-seq data and yolk sac EMP scRNA-seq data was obtained from EMBL-EBI Array Express with experiment codes E-MTAB-6701 and the Gene Expression Omnibus (GEO) under the accession number GSE137117.

QUANTIFICATION AND STATISTICAL ANALYSIS

GraphPad Prism 6 was used to analyze the data. The data are reported as the mean ± s.d.. A Student's unpaired two-tailed *t* test was applied for the statistical.